Analytica Chimica Acta 1201 (2022) 339634

Contents lists available at ScienceDirect

Analytica Chimica Acta

journal homepage: www.elsevier.com/locate/aca

Ultra-sensitive speciation analysis of tellurium by manganese and iron assisted photochemical vapor generation coupled to ICP-MS/MS

Eva Jeníková [a, b, *], Eliška Nováková [a, b], Jakub Hraníček [a], Stanislav Musil [b]

[a] Charles University, Faculty of Science, Department of Analytical Chemistry, Albertov 6, 128 43, Prague, Czech Republic
[b] Institute of Analytical Chemistry of the Czech Academy of Sciences, Veveří 97, 602 00, Brno, Czech Republic

HIGHLIGHTS

- Mn^{2+} used as sensitizer in PVG from acetic and formic acid medium for the first time.
- Mn^{2+} and Fe^{2+} enhanced PVG efficiency to ≈50% in a simple Teflon coiled reactor.
- LOD of 1.3 ng L^{-1} obtained by PVG-ICP-MS/MS using 128 *m/z* and O_2 mode (+16 *m/z*).
- A feasibility of non-chromatographic speciation analysis of Te^{4+} and Te^{6+} demonstrated.
- Excellent tolerance to inorganic anions enabled Te determination even in seawater.

GRAPHICAL ABSTRACT

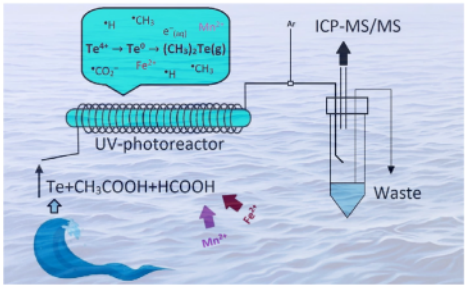

ARTICLE INFO

Article history:
Received 3 November 2021
Received in revised form
3 February 2022
Accepted 17 February 2022
Available online 21 February 2022

Keywords:
Tellurium
Photochemical vapor generation
Atomic absorption spectrometry
Inductively coupled plasma mass spectrometry
Speciation analysis

ABSTRACT

Photochemical vapor generation (PVG) of Te^{4+} was undertaken with a simple reactor consisting of a polytetrafluoroethylene reaction coil wrapped around a low-pressure mercury tube lamp and using a flow-injection for sample delivery. The composition of a reaction medium, the influence of irradiation time and the effect of added sensitizers and interferents were investigated using high-resolution continuum source atomic absorption spectrometry and a miniature diffusion flame atomizer. A mixture of 5 M acetic acid and 3.5 M formic acid and sample flow rate of 4 mL min^{-1} permitting a 36 s irradiation time were found optimal for PVG of Te^{4+}. The addition of 250 mg L^{-1} Mn^{2+} and 15 mg L^{-1} Fe^{2+} ions as sensitizers enhanced the overall PVG efficiency 2.75-fold to 50 ± 2%. In order to achieve higher sensitivity necessary for determination of Te in real environmental samples, PVG was coupled to inductively coupled plasma triple quadrupole mass spectrometer and detection was performed with O_2 in the reaction cell utilizing a mass shift mode of measurement (*m/z* 128 → *m/z* 144) to ensure interference free ion detection. A limit of detection 1.3 ng L^{-1} and repeatability (RSD) 0.9% at 250 ng L^{-1} were achieved. This ultrasensitive methodology was validated for speciation analysis of Te in water samples of various matrix complexities (fresh water, well water, seawater and contaminated water). Since no response was observed from Te^{6+} under optimal PVG conditions, Te^{4+} was selectively determined by direct PVG. The sum of Te^{4+} and Te^{6+} was determined after pre-reduction of Te^{6+} in 6 M HCl (95 °C), evaporation to dryness and reconstitution in the reaction medium containing sensitizers. Very good accuracy was

* Corresponding author. Charles University, Faculty of Science, Department of Analytical Chemistry, Albertov 6, 128 43, Prague, Czech Republic.
E-mail address: jenikoev@natur.cuni.cz (E. Jeníková).

https://doi.org/10.1016/j.aca.2022.339634

demonstrated by spiked recoveries for both Te^{4+} and total Te in water samples and also by total Te determination in fresh water Standard Reference Material NIST 1643f.

1. Introduction

Exposition of human to higher concentrations of Te may negatively affect kidneys, nervous system, lungs and gastrointestinal tract [1]. Although tellurium is very rare in the environment, its use has rapidly increased due to applications in emerging technologies such as semiconductors in solar power industry [2–4]. This is why it has been included in the newly established group of so-called technology-critical elements [5]. There is an increasing demand for the development of unique analytical methodologies for ultra-trace determination and speciation analysis, which will provide us with the possibility of monitoring changes in the concentration of tellurium and its species caused by anthropogenic activities in order to eliminate possible negative effects on humans. Unfortunately, there is very little information about naturally occurring concentrations of tellurium in the environment and even less about speciation of this element [3].

Currently, inductively coupled plasma mass spectrometry (ICP-MS) using conventional pneumatic nebulization (PN) of solutions serves as a method of choice for sensitive determination of elements, although its detection capability in terms of limit of detection (LOD) remains insufficient to access naturally occurring levels of Te in environmental samples (in single to maximum low tens of ng L^{-1}) [3]. The main challenges related to detection with a single quadrupole ICP-MS are the high 1st ionization potential of Te (9.01 eV) and the existence of a number of stable isotopes plagued by interferences. The recommended mass of *m/z* 125 offers natural abundance of only 7.1% resulting in low sensitivity of measurement while much more abundant isotopes at *m/z* 126 (18.8%), *m/z* 128 (31.7%) and *m/z* 130 (34.1%) are plagued by isobaric interferences from Xe^{+} and Ba^{+}. A new strategy to control isobaric interferences is the use of inductively coupled plasma mass spectrometer with triple quadrupole (ICP-MS/MS) and employing O_2 or NH_3 reaction mode and mass shift.

A substantial improvement in detection capabilities can be provided by vapor generation (VG), which can significantly increase the efficiency of the analyte introduction. Hydride generation (HG) is a mature technique enabling also speciation analysis of Te (i.e., inorganic Te^{4+} and Te^{6+} species that occur in the environment almost exclusively [3]). It is well known that Te^{4+} efficiently generates TeH_2 upon HG while Te^{6+} does not, so pre-reduction is very important for the possibility of determination of total Te in samples [6].

Photochemical vapor generation (PVG) is an alternative VG technique gradually gaining in importance. The mechanism of PVG is based on photodecomposition of low molecular weight organic acids by UV radiation and formation of radicals such as $H^{\bullet}$, $R^{\bullet}$ and $COO^{\bullet-}$ and hydrated electrons ($e^{-}(aq)$) [7,8]. These radical species interact with elements of interest to form volatile compounds, e.g., hydrides, carbonyl or alkyl compounds, depending on the reaction medium used [9]. Generated volatile compounds are efficiently separated from the sample matrix and transported with high efficiency to any atomic spectrometry detector. Recently, introduction of new photocatalysts (TiO_2) [10] and especially some transition metal ion sensitizers have constituted a new impulse for development of PVG methodology and its expand to new analytes, including metals, metalloids and even non-metals [11–20].

The feasibility of PVG of Te was firstly demonstrated by Guo et al. [8] using a batch style UV reactor. This pioneer paper was followed by more in-depth but still multi-element studies [21–23] using various flow arrangements of the PVG generators and low molecular organic weight acids as reaction media (formic acid or mixture of formic and acetic acid). Transition metal ions have been also employed as sensitizers to substantially enhance the efficiency of PVG of Te^{4+}. He et al. [24] demonstrated a strong synergistic effect of $Fe^{2+/3+}$ ions and nano-TiO_2 on PVG of Te^{4+} from a mixture of acetic and formic acid using a thin-film flow-through quartz photoreactor. Besides, the use of nano-TiO_2 provided efficient PVG from Te^{6+} species, resulting in equal PVG efficiency and thus sensitivity as for Te^{4+}. Very recently, Co^{2+} ions added to the mixed medium (acetic and formic acid again) have been shown to exhibit even greater enhancement effect on PVG of Te^{4+} than $Fe^{2+/3+}$ ions, when used without TiO_2, employing the same reactor [17].

In this work we aimed to optimize conditions of PVG of Te^{4+} using a simple PTFE reactor coiled around a standard Hg low-pressure tube lamp and investigate an effect of various metal sensitizers or their combinations to achieve as high overall PVG efficiency as possible. Subsequently, we focused on the coupling of PVG with ICP-MS/MS to obtain detection power that would enable Te determination in natural or slightly contaminated water samples. This included also a validation of a non-chromatographic scenario for speciation analysis of Te.

2. Experimental

2.1. Reagents and chemicals

Deionized water (<0.2 μS cm^{-1}, Ultrapur, Watrex, USA) was used for preparation of all solutions. A stock solution of 1000 mg L^{-1} of Te^{4+} in ≈2.4 M HCl was sourced from Analytika (Czech Republic) while 1000 mg L^{-1} of Te^{6+} (as telluric acid) from BDH (UK). Acetic acid (≥99.5%, Sigma-Aldrich, USA) and formic acid (≥98%, Merck, Germany) were used for preparation of the reaction media and these solutions were prepared fresh daily. Stock solutions of potential sensitizers were prepared from following compounds: cadmium(II) acetate tetrahydrate (p.a., Lach-Ner, Czech Republic), cobalt(II) acetate tetrahydrate (p.a., Lach-Ner, Czech Republic), copper(II) acetate monohydrate (p.a., Merck, Germany), iron(II) acetate (≥99.99%, Sigma-Aldrich, USA), manganese(II) acetate tetrahydrate (p.a., Sigma-Aldrich, USA), nickel(II) acetate tetrahydrate (p.a., Sigma-Aldrich, USA), sodium tungstate(VI) dihydrate (p.a., Merck, Germany). Other chemicals were sourced as follows: nitric acid (65%, semiconductor grade) from Honeywell (USA); hydrochloric acid (37%, p.a.), sodium nitrate and sodium sulfate from Merck (Germany); sulfuric acid (98%, p.a.) from Lach-Ner (Czech Republic); and sodium chloride from Lachema (Czech Republic). Three Certified Reference Materials (CRM) were used in this study: NIST SRM 1643f (Trace Elements in Water), CASS-5 (Nearshore Seawater Reference Material for Trace Metals) and NASS-7 (Seawater Certified Reference Material for Trace Metals and other Constituents).

2.2. Instrumentation

A PVG system based on flow injection (FI) mode of operation

similar to that described in our previous study [13] was employed (Fig. 1). Almost all tubing was made of PTFE except for tubes used for pumping of solutions made of Tygon (1.42 mm i.d., Ismatec, Germany). The photoreactor was made of a low-pressure mercury UV bench lamp (20 W, dimensions 610 × 35 mm, Ushio, Japan) placed in a power supply with mirror walls covered with aluminum foil to protect the operator from UV exposure. The circumference of this tube lamp was tightly wrapped with 480 cm long piece of 0.8 mm i.d. x 1.58 mm o.d. PTFE tubing (inner volume ≈2.4 mL) where the sample solution was irradiated. A constant flow of the reaction medium through the photoreactor was maintained by a peristaltic pump (Masterflex, Cole-Parmer, USA). Sample/standard solution was introduced into a stream of the reaction medium using an injection valve (V-451, IDEX Health and Science, USA; sample loop volume 0.5 mL). The outflow from the photoreactor was mixed with a flow of Ar carrier gas, controlled by a mass-flow controller (Cole-Palmer, USA), and carried to a gas-liquid separator (GLS), where the volatile species were separated from the liquid phase. The GLS was a modified polypropylene centrifuge vial with inner volume of 15 mL [13,14] and was immersed in an ice/water bath to reduce the release and transport of formic and acetic acid vapors into the atomizer/plasma. The GLS was connected either to atomic absorption spectrometry (AAS) or ICP-MS/MS via 40 cm long PTFE tubing (2 mm i.d.). Unless explicitly stated otherwise, Ar carrier flow of 250 mL min^{-1} was employed during AAS measurements while 800 mL min^{-1} was employed when the generator was coupled to ICP-MS/MS.

AAS measurements were made using a high-resolution continuum source atomic absorption spectrometer (HR-CS-AAS) ContrAA 300 (Analytik Jena AG, Germany) at 214.281 nm. Three pixels of the CCD array detector corresponding to ≈4.5 pm, were taken for evaluation of peak volume selected absorbance [25]. A commercial nebulization system and a burner were replaced with a miniature diffusion flame atomizer (MDF, detailed in Ref. [13]). It consisted of a vertical quartz tube with 6 mm i.d. and a side inlet for introduction of Ar carrier containing volatile species. The MDF atomizer was supplied at the lower end of the vertical tube with a flow of H_2 (100 mL min^{-1}) that served as a fuel. The MDF atomizer was positioned in such way that the axis of the optical beam would intersect the vertical axis of the quartz tube and the lower edge of the optical beam would be set just above its rim (observation height 0 mm).

An Agilent Technologies 8900 ICP-MS/MS was used for the determination of the overall PVG efficiency, for substantial improvement of LOD and analytical applications. FI-PVG system was coupled to the inlet of a Scott-type spray chamber of the ICP-MS/MS instrument that normally serves as the inlet for makeup Ar [13,14,26,27]. To provide more robust wet plasma conditions and to monitor plasma stability, 2% HNO_3 as a carrier liquid was mixed in a T-piece with a 40 μg L^{-1} Rh in 1% HNO_3 as an internal standard solution (IS) and was subsequently nebulized by a MicroMist nebulizer into the spray chamber concurrently with PVG. The carrier liquid channel was equipped with a manual injection valve (sample loop volume 0.5 mL) and utilized exclusively for determination of overall PVG efficiency (see Section 2.4.). Optimal plasma settings are listed in Table 1. Standard tuning procedure was conducted daily to check the sensitivity of the instrument and was followed by further tuning while concurrently operating with PN and PVG. The transient FI signals were exported as CSV files and manually integrated in MS Excel and corrected for any sensitivity drift relative to changes in IS signal intensity.

With the exception of initial experiments that were performed in standard no gas mode or He collision mode (4.1 mL min^{-1}), the measurements were carried out with O_2 in the reaction/collision cell using a mass shift mode (+16 *m/z*). Tellurium was measured as $^{128}Te^{16}O^+$ at *m/z* 144 and internal standard rhodium (as $^{103}Rh^{16}O^+$) was monitored at *m/z* 119.

Conventional PN-ICP-MS/MS equipped with an Agilent SPS 4 autosampler was employed in the initial evaluation of the suitability of the reaction/collision cell chemistry for Te measurement. Five replicate steady-state measurements were conducted monitoring ^{125}Te, ^{126}Te, ^{128}Te and ^{130}Te isotopes using the reaction/collision cell operating in a standard no gas mode, He mode (4.1 mL min^{-1}) and O_2 mode (45% ≈ 0.45 mL min^{-1}) in the reaction/collision cell (monitoring after a mass shift +16 *m/z* for the O_2 mode). O_2 mode and monitoring ^{128}Te and ^{103}Rh after a mass shift +16 *m/z* were utilized for parallel determination of total Te in real water samples.

UV–vis absorption spectra of the reaction media were recorded with an Agilent 1260 Infinity II variable wavelength detector in the range 190–600 nm using 1 nm steps.

2.3. Treatment of real samples

In addition to three CRMs, four water samples were employed to verify recovery of Te^{4+} and total Te. A well water sample was collected from a local well which is still used as a source of drinking water. Three samples of contaminated water were collected from exploratory wells close to a sludge dump near a chemical factory in the city of Břeclav, Czech Republic (contaminated water I–III). These samples were filtered through a 0.45 μm PTFE syringe filter and prepared for parallel analysis using (i) conventional PN-ICP-

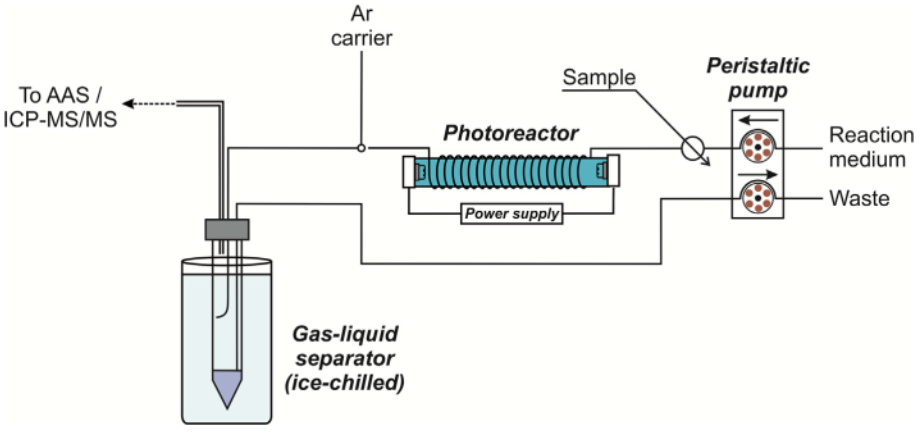

Fig. 1. Schematic diagram of a photochemical vapor generation system.

Table 1
ICP-MS/MS parameters for coupling with PVG.

RF power	1550 W
RF matching	1.20 V
Sampling depth	8 mm
Dilution Ar	0 mL min^{-1}
Nebulizer Ar	590 mL min^{-1}
Ar carrier for PVG	800 mL min^{-1}
ICP-MS peristaltic pump flow	0.1 rps (0.31 mL min^{-1} carrier liquid and 0.06 mL min^{-1} IS solution)
Spray chamber temperature	2 °C
Reaction cell gas	O_2 (45% ≈ 0.45 mL min^{-1})
Axial acceleration/Energy discrimination	2.0 V/−7.0 V
Acquisition mode	Time resolved analysis
Scan type	MS/MS
Measured isotopes	Rh (*m/z* 103 → *m/z* 119, 0.05 s),
(Q1→Q2, dwell time)	Te (*m/z* 128 → *m/z* 144, 0.1 s)

MS/MS (prepared in 2% HNO_3) for total Te determination and (ii) FI-PVG-ICP-MS/MS for speciation analysis of Te.

Water samples for Te^{4+} determination were prepared as follows: ≈21 mL of water sample was prepared in 5 M acetic acid and 3.5 M formic acid with the addition of 250 mg L^{-1} Mn^{2+} and 15 mg L^{-1} Fe^{2+} as sensitizers (total volume was always 40 mL) and subjected to direct analysis by FI-PVG-ICP-MS/MS using a standard addition technique for calibration. A pre-reduction in heated HCl (6 M) was used for determination of total Te (i.e., Te^{4+} and Te^{6+}) in water samples. 20 mL of water sample was mixed with 20 mL concentrated HCl in a glass vial, heated and evaporated in a thermoblock at 90–100 °C to dryness. The residue was dissolved in 40 mL of the reaction medium (5 M acetic acid and 3.5 M formic acid containing 250 mg L^{-1} Mn^{2+} and 15 mg L^{-1} Fe^{2+}) and subjected to analysis by FI-PVG-ICP-MS/MS using a standard addition technique.

2.4. Determination of overall PVG efficiency

Overall PVG efficiency was determined according to our previously published procedure [13,14,15,20,28,29] and it is the product of a sensitivity enhancement factor and absolute PN efficiency. The enhancement factor was calculated as the ratio of the sensitivity obtained with FI-PVG sample introduction to that arising from FI-PN during their concurrent operation; hence both calibration curves were measured under exactly the same plasma conditions. The PN efficiency was determined under optimal settings of the ICP-MS/MS (Table 1) using a modified waste collection method, see Refs. [13,14,15,28,29] for details.

2.5. Procedure and conventions

PVG measurements were exclusively conducted in the FI mode when a constant flow of the carrier (reaction) medium was propelled by the peristaltic pump and a standard/sample prepared in the reaction medium containing sensitizers was manually injected into the carrier stream at the beginning of recording of signal; the recording was stopped after the transient signal returned to the baseline. Peak volume selected absorbance evaluated from 3 pixels was employed as a measure of the analyte response in HR-CS-AAS. Peak area (in counts) normalized for the averaged signal from the IS over the same time window was employed as a measure of analyte response in ICP-MS/MS. Each result is presented as the average of at least three replicates with an uncertainty given as ± one standard deviation (SD) or combined SD where results are relative. LOD is calculated as 3 × SD_{blank}/slope of regression of a calibration function. Overall PVG efficiency is defined as the fraction of the analyte that is converted to volatile species, released to the gas phase and transported to the plasma. PN efficiency represents the fraction of analyte introduced into the spray chamber through the nebulizer and transported in the form of aerosol to the plasma.

3. Results and discussion

3.1. Optimization of PVG of Te^{4+} by HR-CS-AAS

The relevant PVG conditions (composition of the reaction medium, irradiation time (IT) and effect of metal sensitizers) leading to the optimized overall PVG efficiency were investigated based on the response from HR-CS-AAS. The MDF atomizer was used for atomization of generated volatile Te species based on our previous positive experience with this type of atomizer during optimization of chemical VG or PVG of various analytes [13,30,31]. The flow rates of Ar carrier and H_2 needed to sustain the flame were kept at 250 mL min^{-1} and 100 mL min^{-1}, respectively, because these conditions provided satisfactory sensitivity and repeatability of HR-CS-AAS measurements (Note: LOD of 3.2 μg L^{-1} and repeatability of 2.4% (n = 10) at 500 μg L^{-1} was achieved at optimal PVG conditions). The effect of Ar carrier on the overall PVG efficiency was not investigated with the MDF atomizer because of serious dilution of free atoms in the observed volume of the flame at higher Ar carrier flow rates, hence, it was investigated separately with ICP-MS/MS detector (see Section 3.3.).

Composition of the reaction medium was the first studied parameter (Fig. 2). A synergistic effect of acetic and formic acid on PVG of Te^{4+} was identified when only a mixture of both acids led to efficient PVG. Absolutely no response was obtained from only formic acid in the range 0–6 M and only negligible response was obtained from acetic acid at concentration 6–8 M. The optimal composition of the reaction medium at 4 mL min^{-1} (corresponding to IT ≈ 36 s) that provided the highest response was 5 M acetic acid and 3.5 M formic acid. Higher concentration of both acids than optimum led to a rapid decrease of response most probably because of the decreased penetration depth of the UV radiation arising from the higher absorptivity of the reaction medium. The importance of the use of the mixture of acetic and formic acid for PVG of Te^{4+} has been highlighted by several authors employing various designs of the photoreactors [17,23,24].

The influence of IT was tested using 5 M acetic acid and 3.5 M formic acid by altering the reaction medium flow rate in the range from 2 mL min^{-1} to 8 mL min^{-1} (IT ≈ 18–72 s). No distinct maximum of the response was observed in the range 4–7 mL min^{-1} (IT ≈ 21–36 s) because the response was still within 90–100% range. The flow rate of 4 mL min^{-1} which corresponds to an IT of approximately 36 s was chosen for further experiments to eliminate excess consumption of the reaction medium.

The possibility of substantial enhancement in overall PVG efficiency was investigated by addition of various metal ion sensitizers to 0.5 mg L^{-1} Te^{4+} in a mixture of 5 M acetic acid and 3.5 M formic acid and (Fig. 3). Metal ions (Co^{2+}, Fe^{2+}, Cu^{2+}, Ni^{2+} and Cd^{2+}) were chosen on the basis of their previously reported effect on PVG of Te^{4+} [17,24] and other analytes (see Ref. [19]). In addition to these ions, Mn^{2+} and W^{6+} were examined. The sensitizers were added in the form of acetate or in the case of W^{6+} in the form of sodium tungstate to avoid addition of nitrate or chloride into the reaction medium, because these anions can cause serious interference during PVG (see Section 3.2.).

It is evident in Fig. 3 that the addition of Mn^{2+} and Fe^{2+} led to the highest enhancement of the response − 2.37 and 1.96–fold, respectively, at the optimal concentrations of 250 mg L^{-1} Mn^{2+} and 15 mg L^{-1} Fe^{2+}. No positive effect of added Ni^{2+} and W^{6+} was observed as well as for Co^{2+}, which is not in line with the work by Zeng et al. [17] who described a crucial enhancement at 1 mg L^{-1}

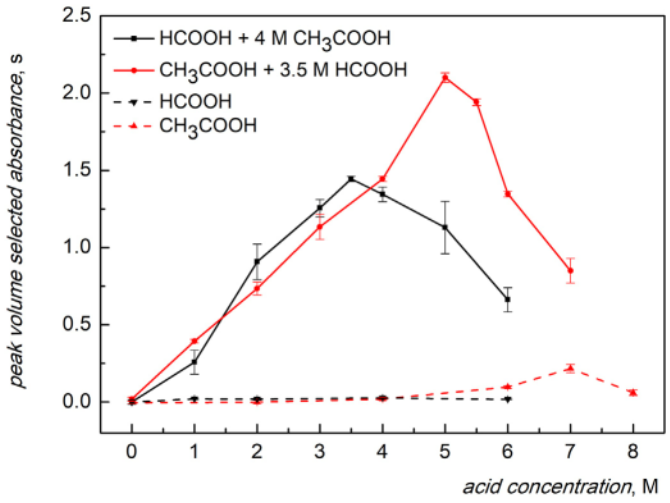

Fig. 2. Effect of the composition of reaction medium on FI-PVG-HR-CS-AAS response from 1 mg L^{-1} Te^{4+} at reaction medium flow rate 4 mL min^{-1}; black dash line – effect of formic acid; black solid line – effect of formic acid at 4 M acetic acid; red dash line – effect of acetic acid; red solid line – effect of acetic acid at 3.5 M formic acid. (For interpretation of the references to colour in this figure legend, the reader is referred to the Web version of this article.)

Co^{2+} (13-fold). The enhancement in overall PVG efficiency by added Fe^{2+} in our work (almost 2-fold) was also not so substantial as reported by Zeng et al. [17] and He et al. [24] (5–6-fold). This may be due to the difference in the PVG generators used (PTFE coiled reactor vs. quartz thin-film flow-through [17,24]), permitting access to emitted wavelengths (254 nm vs. 185 and 254 nm), or the state of optimization of PVG without added sensitizers. If very low overall PVG efficiency (in single percent units) is achieved without the sensitizer(s), then addition of sensitizer can lead to even more than 10-fold enhancement.

Cd^{2+} and Cu^{2+} ions had a detrimental effect on PVG of Te^{4+} at concentrations as low as 0.5 mg L^{-1}. Tellurium may form CdTe in the presence of Cd^{2+} under UV irradiation, similarly as Se forms CdSe [32], resulting in the loss of Te^{4+} species available for PVG. A very similar "scavenging" effect, but with an opposite role of the analyte and interferent, was also reported for PVG of Cd^{2+} in the presence of Se^{4+} and Te^{4+} or Te^{6+} ions recently [15,33]. The highly negative effect of Cu^{2+} is not clear but is analogous to that observed

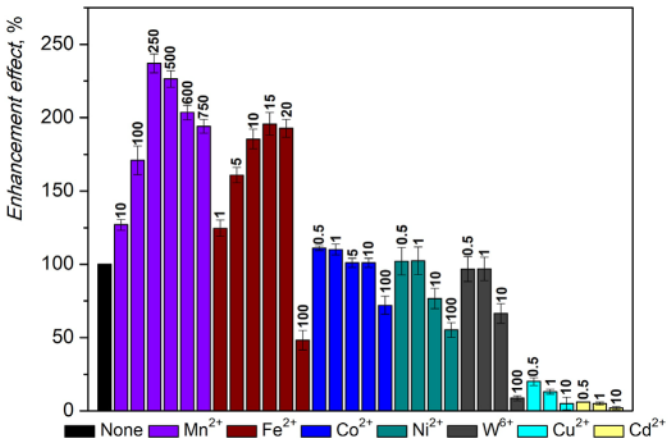

Fig. 3. Enhancement effects of various concentrations of added sensitizers (in mg L^{-1}) on FI-PVG-HR-CS-AAS response; experimental conditions: 0.5 mg L^{-1} Te^{4+}, 5 M acetic acid and 3.5 M formic acid, reaction medium flow rate 4 mL min^{-1}; relative to the response obtained at PVG conditions without added sensitizer (100%, black column).

by He et al. [24] who attributed it to the formation of a charge neutral tellurium copper colloidal compound during PVG. Similarly, Zeng et al. [17] speculated that the serious interference effect of Cu^{2+} at 20 and 200 μg L^{-1} can be due to the decomposition of volatile compound of Te (identified as dimethyl telluride). They managed to eliminate this interference by masking Cu^{2+} with diethyldithiocarbamate (DDTC).

Noting the significant positive influence of Mn^{2+} and Fe^{2+} ions (Fig. 3), the interaction of both ions on PVG of Te^{4+} was further examined by addition of various concentrations of Fe^{2+} to 250 mg L^{-1} Mn^{2+} and by addition of various concentrations of Mn^{2+} to 15 mg L^{-1} Fe^{2+}. In both cases, a further enhancement by the factor of ≈1.2 and ≈ 1.4, respectively, was associated with maxima at 15 mg L^{-1} Fe^{2+} and 250 mg L^{-1} Mn^{2+}, respectively. The resulting enhancement effect equaled 2.75 ± 0.10-fold compared to the response obtained without addition of any sensitizer. This effect cannot be described as synergistic (i.e., combined effect of both sensitizers that is greater than the cumulative effect that those sensitizers produced when used individually), which was reported for PVG of Re and Ru sensitized with Cd^{2+} and Co^{2+} ions recently [19,20]. The action of two metals is rather "additive" as reported for PVG of Mo sensitized with Co^{2+} and Cu^{2+} ions [34].

Reaction medium consisting of 5 M acetic acid and 3.5 M formic acid with the addition of 250 mg L^{-1} Mn^{2+} and 15 mg L^{-1} Fe^{2+} to the sample/standard was selected for further investigations.

There is definitely a lack of a comprehensive mechanistic interpretation for PVG in general, and more recently that of the impact of added transition metal sensitizers on PVG efficiency remains a shortcoming with studies of PVG [7,9,19]. The effect of the presence of transition metal ions has often been associated with formation of metal formate complexes which change the absorption characteristics of the reaction medium. Such a change may enhance the rate of photo-oxidation of formic acid [7] and/or alter the reaction scheme in favor of production of highly reducing radicals (see below). In this work, we focused on examination of UV–vis absorption spectra of various unphotolysed reaction media with transition metals as sensitizers and analyte and searched for the appearance of any absorption band that could overlay with 254 nm, the main spectral line available in our PTFE coiled reactor. A significant absorption by a mixture of formic acid and acetic acid occurred at wavelength below 260 nm. Formic acid alone exhibited higher absorption than acetic acid at 254 nm, which is consistent with earlier reports [35]. The presence of Te^{4+} and Mn^{2+} (10 and 250 mg L^{-1}, respectively) in the mixture of acetic and formic acid exhibited no change or shift in the spectra while addition of Fe^{2+} ions (15 mg L^{-1}) resulted in the appearance of a significant absorption band having a maximum at ≈285 nm, which corresponds to previous reports again [36,37]. This absorption band is attributed to iron formate/acetate [35] and significantly overlaps with 254 nm line emitted by the low-pressure Hg lamp. It was not influenced by the addition of 250 mg L^{-1} Mn^{2+} and 10 mg L^{-1} Te^{4+}. However, the iron formate/acetate absorption band cannot be fully responsible for the enhancement in PVG of Te^{4+}, which would be in accord with the first law of photochemistry. Convenient absorption band with maximum even closer to 254 nm line was reported for W^{6+} (255–260 nm) [14] and confirmed in this work. Tungsten likely forms tungsten formate/acetate in a mixture of acetic and formic acid, however, addition of W^{6+} ions exhibited absolutely no positive effect on PVG of Te^{4+} (see Fig. 3). Additionally, only the increase in absorptivity of the reaction medium cannot explain the positive effect of Mn^{2+} ions on PVG that resulted in the appearance of no absorption band close to 254 nm line.

The exact nature of the positive effect of Mn^{2+} and Fe^{2+} ions and their combination on PVG of Te^{4+} can be speculated here in the light of recent studies of generated free radicals. UV photolysis of

formic acid yields several radical species (mainly $H^{\bullet}$, $HCOO^{\bullet}$, $HCO^{\bullet}$ and $COO^{\bullet-}$) and $e^{-}(aq)$ while acetic acid brings also $CH_3^{\bullet}$ into play [7,9]. Higher production of highly reducing $COO^{\bullet-}$ during UV irradiation of formic acid in the presence of Co^{2+} and Cu^{2+} ions was demonstrated recently by application of electron paramagnetic resonance (EPR) spin trapping techniques [34]. The same results were subsequently confirmed for PVG of Re using Cd^{2+} and Co^{2+} ions as sensitizers [19] and PVG of Te^{4+} using only Co^{2+} as the sensitizer and a mixture of acetic and formic acid [17]. It is highly probable that the similar enhancement in production of $COO^{\bullet-}$ occurs also in our system sensitized with Mn^{2+} and/or Fe^{2+} ions. Although the role of co-generated $e^{-}(aq)$ and $H^{\bullet}$ should not be neglected, the increased production of $COO^{\bullet-}$ seems to be critical to sequential reduction of Te^{4+} to Te^{0}. This is followed by rapid uptake of $CH_3^{\bullet}$ derived from the photolysis of acetic acid to yield volatile dimethyl telluride.

3.2. Interferences

Considering the application of this methodology for speciation analysis of Te in real samples, the interferences caused by inorganic anions (NO_3^-, SO_4^{2-}, Cl^-) added in the form of acids or sodium salts were investigated with FI-PVG-HR-CS-AAS (Fig. 4). Instead of spiking rather low ppm (i.e., sub mM levels) of interferents, as is common in the majority of PVG studies, we focused on a complete mapping of the effect of inorganic anions and identification of the levels that are still acceptable for accurate Te^{4+} determination. Such knowledge is highly valuable if determination of Te is required from real samples that are stabilized in acids (mainly in HNO_3) or from samples containing high salt content (seawater).

NO_3^- was found to be the most serious interferent wherein concentrations of 25 mM caused a significant decrease in response (by ≈ 30%), most probably due to scavenging of free radicals. The PVG system was more tolerant to the presence of Cl^- and SO_4^{2-} anions that started interfering at much higher concentrations. While the impact of $NaNO_3$ was very similar to that of HNO_3, the tolerance towards NaCl was much better than found for HCl, most probably due to change in pH of the reaction medium – a significant decrease in response (by 22%) was observed for 500 mM of NaCl while 15% decrease in response was obtained with 200 mM HCl. Such tolerance towards NaCl seems to make a direct determination of Te^{4+} by PVG in seawater feasible (see Section 3.5.).

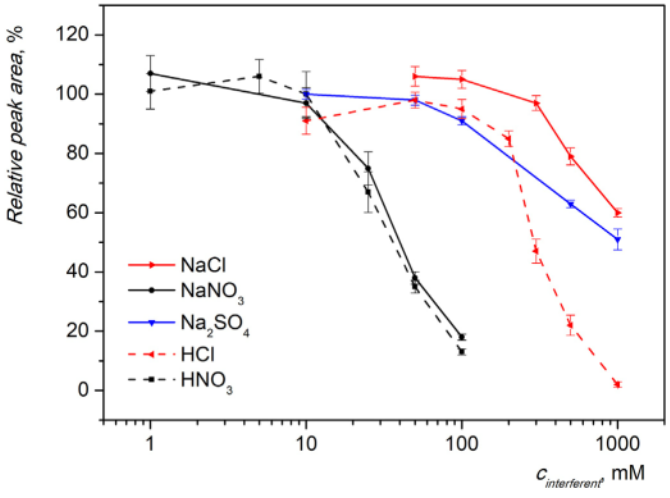

Fig. 4. Relative effects of added interferences on FI-PVG-HR-CS-AAS response of 0.5 mg L^{-1} Te^{4+}; experimental conditions: 5 M acetic acid and 3.5 M formic acid containing 250 mg L^{-1} Mn^{2+} and 15 mg L^{-1} Fe^{2+}, reaction medium flow rate 4 mL min^{-1}.

As mentioned above, it is not possible to give any comparison of the tolerance towards interferences from these inorganic anions with the earlier studies because these studies provided insufficient mapping of the effect of such ions at higher than mM levels [17,24]. The only exception is the work by Romanovskiy et al. [23] who provided critical concentrations (> 10% response suppression) for NO_3^- as 1 mg L^{-1} (≈0.016 mM) and for SO_4^{2-} as 0.1 mg L^{-1} (≈0.001 mM). These values are three orders of magnitude or even lower than obtained in our work.

3.3. Coupling PVG with ICP-MS/MS

The FI-PVG system was coupled to ICP-MS/MS via an inlet typically used for admitting makeup gas into the spray chamber. Simultaneous PN of a liquid IS and 2% HNO_3 into the spray chamber creates more robust (wet plasma) conditions in the ICP [26], permits the monitoring/correction of any sensitivity drift due to changes in the plasma or interface transmission efficiency and also facilitates determination of the overall PVG efficiency by means of comparison of measured sensitivities obtained with FI-PN and FI-PVG [13,14,20].

An initial evaluation of the suitability of the reaction/collision cell chemistry, i.e., standard no gas mode, He mode (4.1 mL min^{-1}) or O_2 mode (45% ≈ 0.45 mL min^{-1}), was carried out with conventional PN-ICP-MS/MS employing a continuous flow mode (steady-state measurements) and calibration standards 0–10000 ng L^{-1} Te^{4+} in 2% HNO_3. Each mode as well as Te isotopes with higher natural abundance (i.e., ^{125}Te, ^{126}Te, ^{128}Te and ^{130}Te) were evaluated with respect to measured sensitivity and blank that in addition to Te contamination includes the contribution of any polyatomic and isobaric interferents. The latter applies to ^{126}Xe (natural abundance of 0.09%), ^{128}Xe (1.92%) and ^{130}Xe (4.08%) that may be present as an impurity in Ar gas and ^{130}Ba (0.11%) that may be a contaminant in nebulized solutions. In the case of O_2 mode, the isotopes were measured in the mass shift mode (+16 *m/z*). An analogous experiment was subsequently performed with FI-PVG-ICP-MS/MS at optimized conditions. In both the cases, ^{125}Te (recommended mass) in no gas mode and ^{128}Te measured in O_2 mode after mass shift (+16 *m/z*) exerted the best ratios of measured sensitivity and blank, followed by ^{130}Te measured in O_2 mode after mass shift that exhibited only slightly worse ratio. O_2 mode and indirect measurement of ^{128}Te at *m/z* 144 after mass shift was chosen for further experiments to ensure interference free ion detection during real sample analysis. (Note: The sensitivity of ^{128}Te measured in O_2 mode after mass shift was ≈70% of the sensitivity of ^{125}Te measured in standard no gas mode.) Rhodium (1st ionization potential of 7.46 eV) and Ge (7.90 eV) were tested as IS (both measured in the mass shift mode at *m/z* 119 and 88 as $^{103}Rh^{16}O$ and $^{72}Ge^{16}O$, respectively). Rhodium was found to provide slightly better capabilities to correct for intra-day sensitivity drifts and was thus used further. The choice of Rh as the IS in a mass shift mode, with such a different *m/z* value and 1st ionization potential from Te (9.01 eV), may be justified based on the recent conclusions by Bolea-Fernandez et al. [38] which downplay the importance of the roles of mass number and ionization energy for choice of analyte/IS pair in ICP-MS/MS measurements.

In comparison to the MDF atomizer, ICP-MS easily allows for the use and optimization of higher flow rates of Ar carrier for PVG without loss of sensitivity (free atoms dilution occurs in the MDF at higher total gas flow rates). For this experiment only, the Ar gas stream containing volatile Te species leaving the GLS was mixed with an additional flow of Ar in a T-piece placed just before introduction into the spray chamber of ICP-MS. Special care was taken to keep the total gas flow to the spray chamber and to the plasma the

same throughout the experiment, so as to not influence conditions in the plasma or alter sampling depth. Hence, when Ar carrier flow rate (added for PVG through a T-piece between the photoreactor and GLS, see Fig. 1) was increased, the flow rate of additional Ar was decreased accordingly and vice versa. Employing 400 mL min^{-1} for the nebulizer Ar enabled testing the effect of carrier Ar up to 1000 mL min^{-1} (≈1400 mL min^{-1} in total). A parabolic relationship of FI-PVG-ICP-MS/MS response from 5 μg L^{-1} Te^{4+} on Ar carrier flow rate in the range 100–1000 mL min^{-1} was evident. The maximum response with plateau was obtained in the range 800–1000 mL min^{-1}, being some 3.7-fold, 1.6-fold and 1.1-fold higher than that at 100, 250 and 500 mL min^{-1}, respectively. Since the plasma conditions were kept constant during this experiment, including the transport of aerosol carrying IS for sensitivity correction, changes in peak area response reliably reflected changes in the overall PVG efficiency. This result thus suggests either low stability of the generated dimethyl telluride or, more likely, a poor release from the liquid phase at low Ar carrier flow rates. 800 mL min^{-1} Ar carrier was selected for further experiments.

As presented in Fig. 3, Cu^{2+} ions were found to seriously interfere with PVG of Te^{4+} conducted at 250 mL min^{-1} Ar carrier without metal ion sensitizers, wherein a decrease of HR-CS-AAS response to 20 ± 3%, 13 ± 2% and 5 ± 4% was evident at Cu concentration of 0.5, 1 and 10 mg L^{-1}, respectively. We and other authors [17,24] speculated whether it was due to the formation of a tellurium copper colloidal compound during PVG or due to decomposition of volatile dimethyl telluride (see Section 3.1). Regarding a significant change in Ar carrier flow rate required for coupling PVG with ICP-MS/MS, which substantially enhanced the release of volatile species, the effect of Cu^{2+} ions on PVG of Te^{4+} (1 μg L^{-1}) was reinvestigated without and with Mn^{2+} and Fe^{2+} ions sensitizers and compared to that presented in Fig. 3. The recoveries at 0.5, 1 and 10 mg L^{-1} Cu^{2+} corresponded to 102 ± 4%, 79 ± 2% and 40 ± 1%, respectively, for PVG conducted without sensitizers and to 41 ± 1%, 32 ± 2% and 14 ± 1%, respectively, for PVG in the presence of Mn^{2+} and Fe^{2+}. Since the residence time of dimethyl telluride in the condensed phase is minimized at enhanced Ar flow rate, based on these results, the Cu^{2+} interference can be likely ascribed to the decomposition of generated dimethyl telluride.

3.4. PVG efficiency and figures of merit

Overall PVG efficiency and analytical characteristics of FI-PVG-ICP-MS/MS were determined using optimal conditions of PVG (5 M acetic acid and 3.5 M formic acid with 250 mg L^{-1} Mn^{2+} and 15 mg L^{-1} Fe^{2+} added to standard/blank, reaction medium flow rate of 4 mL min^{-1}). Overall PVG efficiency was determined from a comparison of sensitivities obtained using FI mode of analyte introduction with PVG and with conventional PN, both simultaneously coupled to ICP-MS/MS. Detailed description is given in our previous publications [13–15]. Employing 0, 2, 6 and 20 μg L^{-1} Te^{4+} standards for FI-PVG and 0, 10, 40 and 100 μg L^{-1} Te^{4+} standards for FI-PN, the enhancement factor determined as a ratio of slopes of calibrations reached 12.95 ± 0.41. PN efficiency was determined using a modified waste collection method following a recently reported procedure [13–15,20,28,29] as 3.84 ± 0.01% and overall PVG efficiency thus reached 49.8 ± 1.6%. Significantly lower PN efficiency obtained in this work in comparison to our previous papers (≈8%) [13–15,20,28,29] is given by much lower nebulizer Ar flow rate (≈600 mL min^{-1} in this work vs. 1050–1150 mL min^{-1}), which was found optimal in combination with high Ar carrier flow rate required for efficient PVG (800 mL min^{-1}).

Some authors also attempted to estimate/determine the (overall) PVG efficiency of Te. Zheng et al. [21] estimated the PVG efficiency of Te^{4+} generated from formic acid in a reactor made of a quartz tube wrapped around a high-pressure UV lamp in the range 20–30%. They compared the analytical sensitivity obtained with PVG coupled to atomic fluorescence spectrometry (AFS) to that of HG-AFS assuming the efficiency of HG is 100% but no evidence for this value was provided. Using nano-TiO_2 they estimated the efficiency of 20% for PVG of Te^{6+}. He et al. [24] reported excellent PVG efficiency of 91 ± 2% for PVG of both Te^{4+} and Te^{6+} in the thin-film flow-through photoreactor employing 20% (v/v) acetic acid, 2% (v/v) formic acid and 5 g L^{-1} nano-TiO_2 as the reaction medium sensitized with 20 mg L^{-1} Fe^{2+}. They relied on an indirect approach based on the comparison of the signal intensities of Te solutions before and after PVG using HG-AFS when the PVG efficiency is evaluated from the difference of determined concentrations. However, the PVG efficiency determined in this way does not have to really reflect the fraction of an analyte introduced to the detector because this approach may neglect any analyte loss in the apparatus parts. Such an overestimation of PVG efficiency was for example demonstrated for PVG of Cd^{2+} [15] while no substantial losses were identified for PVG of Se^{4+} [39] and Ni^{2+} [40] previously. Nevertheless, we believe that the overall PVG efficiency attained by means of the direct comparison with an alternative sample introduction technique (nebulization) with accurately determined efficiency provides a more reliable image of the state of optimization of PVG. In the light of that, the value of 50% achieved in our simple PTFE coiled reactor can be considered as quite fair efficiency.

The repeatability of FI-PVG-ICP-MS/MS measurements expressed as the relative standard deviation (RSD) of peak areas of a standard of 250 ng L^{-1} was 0.9% (n = 12). The calibration function constructed with 0, 20, 80, 250, 1000 and 2500 ng L^{-1} Te^{4+} standards was linear (R^2 = 0.9987). The relative and absolute LOD (3σ, n = 13) were 1.3 ng L^{-1} and 0.66 pg, respectively. A typically persistent peak-shaped blank signal was obtained and it corresponded to ≈3–4 ng L^{-1} Te^{4+} at the best. Sub-boiling distillation of formic and acetic acid and using an ultrapure water from a commercial supplier (Analpure Ultra, Analytika) provided no improvement, hence, this low blank originates from added sensitizers, most probably from solid manganese(II) acetate, which is present in the reaction medium in high concentration. An estimation of an instrumental LOD, not influenced by Te^{4+} contamination from the added sensitizers, was carried out to illustrate the ultimate potential of the developed FI-PVG methodology. For this, only reaction medium (mixture of 5 M acetic acid and 3.5 M formic acid) was continuously pumped through the photoreactor but the UV lamp was off during measurements of the blank signal. The resultant instrumental LOD obtained in this way was thus dependent only on plasma background and any potential Te contaminant in the nebulized solutions (2% HNO_3 and IS solution) and reached 0.8 ng L^{-1} (3σ, n = 10), which is not so far from the real LOD.

3.5. Application to real samples and speciation analysis of Te^{4+} and Te^{6+}

Analytical applications carried out in PVG studies have been mainly focused on determination of Te^{4+} in real water samples [17,21] or the target oxidation state was even not defined at all [22,23]. The exception is a paper by He et al. [24] who reached efficient PVG from both Te^{4+} and Te^{6+} species by using nano-TiO_2 photocatalyst in combination with Fe^{2+} or Fe^{3+} ions as the sensitizer, which was subsequently validated for determination of total Te content. Nevertheless, speciation analysis of Te^{4+} and Te^{6+} using PVG has not been reported yet.

In this study, negligible response (≤3%) from Te^{6+} was measured using optimal conditions of PVG in comparison to response from Te^{4+}, which can be also to some extent on the account of impurity of Te^{4+} in the Te^{6+} standard stock solution. Hence, the non-

Table 2
Determination of Te^{4+} and total Te (in ng L^{-1} presented with SD) dissolved in water samples by FI-PVG-ICP-MS/MS and determination of total Te by conventional PN-ICP-MS/MS.

Sample	PVG, no pre-reduction		PVG, with pre-reduction		conventional PN
	Te^{4+}	Recovery[a] *(Spiked conc.)*	Total Te	Recovery[a] *(Spiked conc.)*	Total Te (certified)
SRM NIST 1643f	–[b]	–[b]	988 ± 5	95 ± 1 *(0, 500, 2000)*	946 ± 52 (977 ± 8.4)
Well water	<2.5[c]	100 ± 2 *(0, 50, 100)*	–[b]	–[b]	3.1 < x < 10.3[d]
Contaminated water I	19 ± 2	103 ± 4 *(0, 250, 500)*	134 ± 5	114 ± 3 *(0, 250, 500)*	136 ± 8
Contaminated water II	45 ± 5	107 ± 5 *(0, 250, 500)*	398 ± 4	113 ± 2 *(0, 250, 500)*	357 ± 17
Contaminated water III	16 ± 1	106 ± 4 *(0, 250, 500)*	342 ± 5	121 ± 2 *(0, 250, 500)*	337 ± 32
CASS-5	–[b]	–[b]	<5.7[e]	109 ± 1 *(0, 250, 500)* 109 ± 3 *(0, 500, 1000)*[f]	–[b]
NASS-7	–[b]	–[b]	<5.7[e]	112 ± 1 *(0, 250, 500)*	–[b]

[a] Spike recovery for Te^{4+} = slope of standard additions to a sample prepared in the reaction medium with sensitizers)/slope of external calibration × 100 (%); uncertainty evaluated by propagation of error of slopes.
[b] Not determined.
[c] LOD = 2.5 ng L^{-1} (1.3 ng L^{-1} corrected for dilution factor of ≈1.9 introduced by preparation of water sample in the reaction medium).
[d] LOD = 3.1 ng L^{-1}; LOQ = 10.3 ng L^{-1}; calculated from 11 consecutive blanks measured in O_2 mode (*m/z* 128 → *m/z* 144).
[e] LOD = 5.7 ng L^{-1} (3.0 ng L^{-1} corrected for dilution factor of ≈1.9 introduced by preparation of water sample in the reaction medium); calculated from variation of 5 values of peak area of blanks (deionized water) pre-reduced in 6 M HCl.
[f] Spike recovery for Te^{6+}, Te^{6+} spiked prior to pre-reduction.

chromatographic speciation analysis based on the "selectivity" of PVG seemed to be feasible according to the following scenario: 1) Te^{4+} determined directly in one aliquot after addition of the reaction medium with sensitizers; 2) total Te (i.e., Te^{4+} and Te^{6+}) determined by PVG from the other aliquot after its efficient pre-reduction. Concentration of Te^{6+} can be calculated from the difference of concentrations found in both aliquots.

Although several pre-reduction agents have been described in literature [6], pre-reduction of Te^{6+} to Te^{4+} is definitely a challenging task [3]. Heating samples/standards in 6 M HCl for 30–60 min is reliable and the most common procedure preceding determination of total Te by HG technique [6,28]. Since HCl, but also NaCl, were found to interfere at concentrations of > 200 mM and > 500 mM, respectively, the sample pre-reduction procedure was modified to eliminate this interference. Water samples were mixed (1:1) with concentrated HCl and heated in the thermoblock at 90–100 °C until the samples were evaporated to dryness (approximately 19 h). The residue was subsequently dissolved in the reaction medium containing sensitizers and analyzed for total Te content.

A very limiting factor that complicates the verification of accuracy of the developed methodologies is a lack of suitable (water) CRMs with certified total Te content. Moreover, no CRMs are available for Te^{4+} and Te^{6+} species. SRM NIST 1643f (fresh water) provides a certified value of total Te of 977.0 ± 8.4 ng L^{-1} but this is rather too high in comparison to expected levels of Te in natural or only slightly contaminated water samples [3]. The practical feasibility of speciation analysis of Te was thus examined by undertaking FI-PVG-ICP-MS/MS analysis of several water samples and CRMs with various complexity of their matrix (fresh water, well water, seawater, contaminated water) using a standard additions technique (Table 2). The contaminated water samples I–III contained significantly higher concentrations of heavy metals and especially of As (≈3 mg L^{-1}) that was evident from a rapid semiquantitative analysis accompanying the parallel determination made during PN sample introduction. The recoveries were calculated from the ratio of slopes of the Te^{4+} standard additions (no addition and two concentrations) versus external calibration functions. In addition to recoveries, the accuracy was verified by comparison with total Te content certified in SRM NIST 1643f or determined by conventional PN-ICP-MS/MS using O_2 in the reaction cell, ^{128}Te isotope and a mass shift mode (+16 *m/z*).

Excellent recovery in the range 100–107% was obtained for Te^{4+}. CRMs were not analyzed for Te^{4+} because these materials are stabilized in HNO_3 (SRM NIST 1643f in 0.32 M HNO_3, CASS-5 and NASS-7 in ≈0.025 M HNO_3) and because no significant amount of Te^{4+} was previously determined in SRM NIST 1643f suggesting that majority of Te is in the form of Te^{6+} [28]. HNO_3 used for stabilization of CRMs represents an obstacle for PVG because serious interference was observed at 25 mM (see Fig. 4). Despite recent attempts to negate NO_3^- interference [41,42] there is no simple and universal solution and a dilution or evaporation of sample to dryness and its reconstitution with the reaction medium is usually employed. Sample evaporation is covered in the pre-reduction procedure used in this work, motivated especially to remove HCl used for pre-reduction, but it seems to be also effective in a removal of HNO_3. This can be supported by 95–112% recoveries of Te^{4+} added to three pre-reduced CRMs.

The complete (100%) pre-reduction of Te^{6+} to Te^{4+} is demonstrated by very good agreement of total Te concentrations obtained with FI-PVG-ICP-MS/MS to total Te concentrations determined by conventional PN-ICP-MS/MS, or certified value of SRM NIST 1643f. No total Te (< LOD) was detected in CASS-5 and NASS-7 seawater samples. This was surprising because Rodushkin et al. [43] recently reported (for the first time) concentrations of 45 ± 6 ng L^{-1} in CASS-5 (and 46–48 ng L^{-1} in NASS-4 and NASS-6 which are not compatible with NASS-7 but similar values could be expected) using sector field ICP-MS after pre-concentration by evaporation and cation exchange chromatographic separation. The authors however admitted that even 2–3 orders of magnitude lower Te

concentrations in natural seawaters had been reported before their study while some other studies matched closer (for all the relevant literature devoted to Te determination in seawater see Ref. [3]). Spiking Te^{6+} standard (500 and 1000 ng L^{-1}) to CASS-5 before pre-reduction led to 109 ± 3% recovery, which proved complete pre-reduction of Te^{6+} to Te^{4+} even in this sample matrix. Furthermore, the total Te concentration well below 6 ng L^{-1} was also confirmed by HG-ICP-MS/MS employing a pre-reduction by $TiCl_3$ (unpublished results). No attempt to analyze these CRMs samples by conventional PN-ICP-MS/MS was made due to high NaCl content which would require high sample dilution or modified PN-ICP-MS/MS conditions (aerosol dilution), further reflected in even more insufficient LOD. Although no Te in seawater CRMs was detected by FI-PVG-ICP-MS/MS, it should be highlighted that the measurement of seawater can be carried out directly after pre-reduction without any dilution except by the reaction medium. This dilution results in ≈0.31 M NaCl that was shown not to interfere with PVG (see Fig. 4).

4. Conclusions

The overall PVG efficiency of 50% was achieved when PVG of Te^{4+} was conducted from a mixture of acetic and formic acid and in the presence of Mn^{2+} and Fe^{2+} ions as sensitizers. To our best knowledge, this is a first report of Mn^{2+} being used as the sensitizer in PVG. In comparison to Co^{2+} and $Fe^{2+/3+}$ ions that were previously reported to enhance PVG of Te^{4+} [17,24], absolutely no co-generation of volatile Mn compound was observed, hence, the long-term analytical performance is not seriously affected by an excessive metal loading of the ICP-MS spectrometer (torch/interface/ion optics).

The feasibility of sensitive speciation analysis of Te^{4+} and Te^{6+} without chromatography was also demonstrated. Dimethyl telluride is selectively generated by PVG only from Te^{4+} while pre-reduction of Te^{6+} to Te^{4+} has to precede the total Te determination. We admit that the employed pre-reduction by HCl may be laborious and time-consuming and further experiments are needed to find a more suitable pre-reductant that is also compatible with direct PVG. Nevertheless, very good LOD, repeatability and accuracy, supported by the measurement in O_2 reaction mode of ICP-MS/MS, were achieved. The FI-PVG-ICP-MS/MS methodology can be applied to various water sample matrices including seawater without significant matrix interference (especially from chlorides). This is a great benefit in comparison to conventional PN-ICP-MS that requires several-fold dilution of seawater samples, which definitely leads to unsatisfactory sensitivity.

Last but not least, all of this has been achieved with a simple PTFE coiled reactor wrapped around the standard germicidal Hg low-pressure tube lamp. Such reactor can be easily fabricated in a laboratory. In comparison to sophisticated quartz thin-film flow-through photoreactors that have been exclusively used for PVG of Te^{4+} in recent years [17,24], the use of simpler and more readily available photoreactors enhances the attractiveness of the PVG technique and was also highlighted in several recent papers [13,44,45].

CRediT authorship contribution statement

Eva Jeníková: Conceptualization, Methodology, Validation, Formal analysis, Investigation, Data curation, Writing – original draft, Visualization. **Eliška Nováková:** Writing – review & editing, Resources. **Jakub Hraníček:** Resources, Funding acquisition. **Stanislav Musil:** Conceptualization, Methodology, Formal analysis, Investigation, Data curation, Writing – original draft, Writing – review & editing, Supervision, Project administration, Funding acquisition, Resources.

Declaration of competing interest

The authors declare that they have no known competing financial interests or personal relationships that could have appeared to influence the work reported in this paper.

Acknowledgements

This research was carried out within the framework of Specific University Research (Project SVV 260560) and with a support of the Grant Agency of Charles University (Project GA UK 516119), the Czech Science Foundation (project 19-17604Y) and the Czech Academy of Sciences (Institutional support RVO: 68081715). We are also grateful to Adrián García-Figueroa for his comparative analysis by means of HG-ICP-MS/MS.

References

[1] L.A. Ba, M. Döring, V. Jamier, C. Jacob, Tellurium: an element with great biological potency and potential, Org. Biomol. Chem. 8 (2010) 4203–4216.
[2] Q. Tan, Y. Pan, L. Liu, S. Shu, Y. Liu, Determination of ultratrace tellurium in water by hydride generation atomic absorption spectrometry using online separation and pre-concentration with nano-TiO2 microcolumn, Microchem. J. 144 (2019) 495–499.
[3] M. Filella, C. Reimann, M. Biver, I. Rodushkin, K. Rodushkina, Tellurium in the environment: current knowledge and identification of gaps, Environ. Chem. 16 (2019) 215–228.
[4] M. Filella, J.C. Rodríguez-Murillo, Less-studied TCE: are their environmental concentrations increasing due to their use in new technologies? Chemosphere 182 (2017) 605–616.
[5] A. Cobelo-García, M. Filella, P. Croot, C. Frazzoli, G. Du Laing, N. Ospina-Alvarez, S. Rauch, P. Salaun, J. Schäfer, S. Zimmermann, COST action TD1407: network on technology-critical elements (NOTICE)—from environmental processes to human health threats, Environ. Sci. Pollut. Res. 22 (2015) 15188–15194.
[6] J. Dědina, D.L. Tsalev, Hydride Generation Atomic Absorption Spectrometry, Wiley and Sons, Inc., Chichester, 1996.
[7] R.E. Sturgeon, Photochemical vapor generation: a radical approach to analyte introduction for atomic spectrometry, J. Anal. At. Spectrom. 32 (2017) 2319–2340.
[8] X. Guo, R.E. Sturgeon, Z. Mester, G.J. Gardner, Vapor generation by UV irradiation for sample introduction with atomic spectrometry, Anal. Chem. 76 (2004) 2401–2405.
[9] D. Leonori, R.E. Sturgeon, A unified approach to mechanistic aspects of photochemical vapor generation, J. Anal. At. Spectrom. 34 (2019) 636–654.
[10] Z. Zou, J. Hu, F. Xu, X. Hou, X. Jiang, Nanomaterials for photochemical vapor generation-analytical atomic spectrometry, Trends Anal. Chem. 114 (2019) 242–250.
[11] J. Zhou, D. Deng, Y. Su, Y. Lv, Determination of total inorganic arsenic in water samples by cadmium ion assisted photochemical vapor generation-atomic fluorescence spectrometry, Microchem. J. 146 (2019) 359–365.
[12] Y. Wang, L. Lin, J. Liu, X. Mao, J. Wang, D. Qin, Ferric ion induced enhancement of ultraviolet vapour generation coupled with atomic fluorescence spectrometry for the determination of ultratrace inorganic arsenic in surface water, Analyst 141 (2016) 1530–1536.
[13] J. Vyhnanovský, D. Yildiz, B. Štádlerová, S. Musil, Efficient photochemical vapor generation of bismuth using a coiled Teflon reactor: effect of metal sensitizers and analytical performance with flame-in-gas-shield atomizer and atomic fluorescence spectrometry, Microchem. J. 164 (2021) 105997.
[14] J. Vyhnanovský, R.E. Sturgeon, S. Musil, Cadmium assisted photochemical vapor generation of tungsten for detection by inductively coupled plasma mass spectrometry, Anal. Chem. 91 (2019) 13306–13312.
[15] E. Nováková, K. Horová, V. Červený, J. Hraníček, S. Musil, UV photochemical vapor generation of Cd from a formic acid based medium: optimization, efficiency and interferences, J. Anal. At. Spectrom. 35 (2020) 1380–1388.
[16] J. Hu, R.E. Sturgeon, K. Nadeau, X. Hou, C. Zheng, L. Yang, Copper ion assisted photochemical vapor generation of chlorine for its sensitive determination by sector field inductively coupled plasma mass spectrometry, Anal. Chem. 90 (2018) 4112–4118.
[17] W. Zeng, J. Hu, H. Chen, Z. Zou, X. Hou, X. Jiang, Cobalt ion-enhanced photochemical vapor generation in a mixed acid medium for sensitive detection of tellurium(iv) by atomic fluorescence spectrometry, J. Anal. At. Spectrom. 35 (2020) 1405–1411.
[18] Y. Gao, M. Xu, R.E. Sturgeon, Z. Mester, Z. Shi, R. Galea, P. Saull, L. Yang, Metal ion-assisted photochemical vapor generation for the determination of lead in environmental samples by multicollector-ICPMS, Anal. Chem. 87 (2015) 4495–4502.
[19] Y. Zhen, H. Chen, M. Zhang, J. Hu, X. Hou, Cadmium and cobalt ions enhanced-photochemical vapor generation for determination of trace rhenium by ICP-

MS, Appl. Spectrosc. Rev. (2021), https://doi.org/10.1080/05704928.2021.1878368.
[20] S. Musil, J. Vyhnanovský, R.E. Sturgeon, Ultrasensitive detection of ruthenium by coupling cobalt and cadmium ion-assisted photochemical vapor generation to inductively coupled plasma mass spectrometry, Anal. Chem. 93 (2021) 16543–16551.
[21] C. Zheng, Q. Ma, L. Wu, X. Hou, R.E. Sturgeon, UV photochemical vapor generation–atomic fluorescence spectrometric determination of conventional hydride generation elements, Microchem. J. 95 (2010) 32–37.
[22] D.P.C. de Quadros, D.L.G. Borges, Direct analysis of alcoholic beverages for the determination of cobalt, nickel and tellurium by inductively coupled plasma mass spectrometry following photochemical vapor generation, Microchem. J. 116 (2014) 244–248.
[23] K. Romanovskiy, M. Bolshov, A. Münz, Z. Temerdashev, M. Burylin, K. Sirota, A novel photochemical vapor generator for ICP-MS determination of As, Bi, Hg, Sb, Se and Te, Talanta 187 (2018) 370–378.
[24] H. He, X. Peng, Y. Yu, Z. Shi, M. Xu, S. Ni, Y. Gao, Photochemical vapor generation of tellurium: synergistic effect from ferric ion and nano-TiO2, Anal. Chem. 90 (2018) 5737–5743.
[25] U. Heitmann, B. Welz, D.L.G. Borges, F.G. Lepri, Feasibility of peak volume, side pixel and multiple peak registration in high-resolution continuum source atomic absorption spectrometry, Spectrochim. Acta, Part B 62 (2007) 1222–1230.
[26] S. Musil, Á.H. Pétursdóttir, A. Raab, H. Gunnlaugsdóttir, E. Krupp, J. Feldmann, Speciation without chromatography using selective hydride generation: inorganic arsenic in rice and samples of marine origin, Anal. Chem. 86 (2014) 993–999.
[27] J. Šoukal, R.E. Sturgeon, S. Musil, Efficient photochemical vapor generation of molybdenum for ICPMS detection, Anal. Chem. 90 (2018) 11688–11695.
[28] K. Bufková, S. Musil, J. Kratzer, P. Dvořák, M. Mrkvičková, J. Voráč, J. Dědina, Generation of tellurium hydride and its atomization in a dielectric barrier discharge for atomic absorption spectrometry, Spectrochim. Acta, Part B 171 (2020) 105947.
[29] L. Sagapova, S. Musil, B. Kodríková, M. Svoboda, J. Kratzer, Effect of additives on cadmium chemical vapor generation and reliable quantification of generation efficiency, Anal. Chim. Acta 1168 (2021) 338601.
[30] J. Šoukal, O. Benada, T. Matoušek, J. Dědina, S. Musil, Chemical generation of volatile species of copper – optimization, efficiency and investigation of volatile species nature, Anal. Chim. Acta 977 (2017) 10–19.
[31] J. Vyhnanovský, J. Kratzer, O. Benada, T. Matoušek, Z. Mester, R.E. Sturgeon, J. Dědina, S. Musil, Diethyldithiocarbamate enhanced chemical generation of volatile palladium species, their characterization by AAS, ICP-MS, TEM and DART-MS and proposed mechanism of action, Anal. Chim. Acta 1005 (2018) 16–26.
[32] F. Xu, Z. Zou, J. He, M. Li, K. Xu, X. Hou, In situ formation of nano-CdSe as a photocatalyst: cadmium ion-enhanced photochemical vapour generation directly from Se(vi), Chem. Commun. 54 (2018) 4874–4877.
[33] Q. Mou, L. Dong, L. Xu, Z. Song, Y. Yu, E. Wang, Y. Zhao, Y. Gao, Integration of cobalt ion assisted Fenton digestion and photochemical vapor generation: a green method for rapid determination of trace cadmium in rice, J. Anal. At. Spectrom. 36 (2021) 1422–1430.
[34] J. Hu, H. Chen, X. Hou, X. Jiang, Cobalt and copper ions synergistically enhanced photochemical vapor generation of molybdenum: mechanism study and analysis of water samples, Anal. Chem. 91 (2019) 5938–5944.
[35] R.E. Sturgeon, P. Grinberg, Some speculations on the mechanisms of photochemical vapor generation, J. Anal. At. Spectrom. 27 (2012) 222.
[36] Y. Yu, Y. Jia, Z. Shi, Y. Chen, S. Ni, R. Wang, Y. Tang, Y. Gao, Enhanced photochemical vapor generation for the determination of bismuth by inductively coupled plasma mass spectrometry, Anal. Chem. 90 (2018) 13557–13563.
[37] Y. Jia, Q. Mou, Y. Yu, Z. Shi, Y. Huang, S. Ni, R. Wang, Y. Gao, Reduction of interferences using Fe-containing metal–organic frameworks for matrix separation and enhanced photochemical vapor generation of trace bismuth, Anal. Chem. 91 (2019) 5217–5224.
[38] E. Bolea-Fernandez, A. Rua-Ibarz, M. Resano, F. Vanhaecke, To shift, or not to shift: adequate selection of an internal standard in mass-shift approaches using tandem ICP-mass spectrometry (ICP-MS/MS), J. Anal. At. Spectrom. 36 (2021) 1135–1149.
[39] M. Rybínová, S. Musil, V. Červený, M. Vobecký, P. Rychlovský, UV-photochemical vapor generation of selenium for atomic absorption spectrometry: optimization and 75Se radiotracer efficiency study, Spectrochim. Acta, Part B 123 (2016) 134–142.
[40] J. Šoukal, S. Musil, Detailed evaluation of conditions of photochemical vapor generation for sensitive determination of nickel in water samples by ICP-MS detection, Microchem. J. 172 (2022) 106963.
[41] G.S. Lopes, R.E. Sturgeon, P. Grinberg, E. Pagliano, Evaluation of approaches to the abatement of nitrate interference with photochemical vapor generation, J. Anal. At. Spectrom. 32 (2017) 2378–2390.
[42] A. Mollo, M. Knochen, Towards the abatement of nitrate interference on selenium determination by photochemical vapor generation, Spectrochim. Acta, Part B 169 (2020) 105875.
[43] I. Rodushkin, C. Paulukat, S. Pontér, E. Engström, D.C. Baxter, D. Sörlin, N. Pallavicini, K. Rodushkina, Application of double-focusing sector field ICP-MS for determination of ultratrace constituents in samples characterized by complex composition of the matrix, Sci. Total Environ. 622–623 (2018) 203–213.
[44] R.M. de Oliveira, D.L.G. Borges, P. Grinberg, Z. Mester, R.E. Sturgeon, Copper-ion assisted photochemical vapor generation of bromide and bromate, J. Anal. At. Spectrom. 36 (2021) 1235–1243.
[45] R.M. de Oliveira, D.L.G. Borges, P. Grinberg, R.E. Sturgeon, High-efficiency photoreductive vapor generation of osmium, J. Anal. At. Spectrom. 36 (2021) 2097–2106.

Monatshefte für Chemie - Chemical Monthly
https://doi.org/10.1007/s00706-022-02954-4

ORIGINAL PAPER

UV-photochemical vapor generation of tellurium in a thin-film photoreactor with fast stripping of volatile compounds

Eva Jeníková[1,2] · Eliška Nováková[1] · Helena Ruxová[1] · Stanislav Musil[2] · Jakub Hraníček[1]

Received: 30 March 2022 / Accepted: 27 June 2022

Abstract

UV-photochemical vapor generation (UV-PVG) of tetravalent tellurium was investigated in a continuous flow mode using a special experimental setup of the photoreactor where the flow of a carrier gas was admitted upstream of the photoreactor. This was reflected in formation of a thin film of the reaction medium, leading to more effective penetration of UV radiation into the liquid medium as well as release of generated volatile compounds of Te. The aim of the study was to investigate the effect of this unconventional PVG arrangement on the optimal conditions and performance of the method. Only 4 mol dm^{-3} acetic acid as the reaction medium at a flow rate of 2.8 cm^3 min^{-1} was found optimal for UV-PVG of Te(IV) in this photoreactor. Addition of H_2 and temperatures higher than 900 °C were required for efficient atomization in a quartz tube atomizer indicating molecular nature of volatile species. The limit of detection and repeatability obtained for the coupling of UV-PVG with a high-resolution continuum source atomic absorption spectrometry (AAS) were 0.85 µg dm^{-3} and 1.2% ($n = 10$) at 250 µg dm^{-3} Te(IV), respectively. The overall generation efficiency of approximately 8% at UV-PVG conditions optimal for AAS measurements was determined. The differences, similarities and performance of the two generator arrangements are discussed.

Graphical abstract

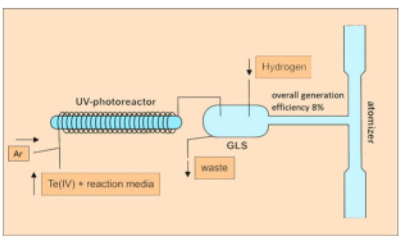

Keywords Photochemistry · Radicals · Vapor generation · Spectroscopy · Tellurium

Introduction

Tellurium is one of the rarest elements. It belongs to the chalcogen group forming oxidation states +4 and +6, therefore, some of its properties are analogous to biogenic elements O, S and Se [1, 2]. However, unlike these elements, Te is toxic and harmful to humans and animals even in low concentrations. Exposition of organisms to Te negatively affects especially kidneys, nervous system, lungs and gastrointestinal tract [3]. Tellurium is still very rare in nature but its use has rapidly increased due to many new applications such as in memory media or solar technologies. This makes

✉ Eva Jeníková
jenikoev@natur.cuni.cz

[1] Department of Analytical Chemistry, Charles University, Faculty of Science, Hlavova 8, 128 43 Prague, Czech Republic

[2] Institute of Analytical Chemistry of the Czech Academy of Sciences, Veveří 97, 602 00 Brno, Czech Republic

Published online: 27 July 2022

this newly defined "technology critical element" a potential environmental hazard unless Te containing products are recycled at the end of their lifetimes [4, 5]. Routine Te determination is usually carried out by atomic spectrometric methods such as atomic absorption spectrometry (AAS), atomic fluorescence spectrometry (AFS) or inductively coupled plasma mass spectrometry (ICP-MS) [6–12] but the detection capabilities have not been typically sufficient to detect naturally occurring contents of Te in the environment.

Vapor generation techniques increase the sensitivity and decrease the limits of detection (LOD) of the above-mentioned atomic spectrometric methods. Among them, chemical hydride generation (HG) has gained a particular importance for routine determination of all hydride forming elements from 14 to 16 groups of the periodic table [13]. UV-photochemical vapor generation (UV-PVG) is a new alternative approach that utilizes UV radiation to convert analytes to volatile compounds [14]. The concept of UV-PVG is environmentally friendly and economical due to the absence of $NaBH_4$ used in HG. Solid $NaBH_4$ is also a common source of analyte contamination, which does not permit to achieve lower LOD. Furthermore, UV-PVG offers very simple instrumentation utilizing only one channel flow setups (in comparison to HG or electrochemical vapor generation) and easy connection with separation methods enabling speciation analysis [15–17].

The heart of a UV-photoreactor is usually a low-pressure mercury lamp irradiating a solution containing the analyte element. The efficiency of UV-PVG is generally the highest from solutions of low molecular weight organic acids (LMWOA), such as formic acid, acetic acid or propionic acid [14, 18–20]. The mechanism of UV-PVG is based on decomposition of such organic compounds by the action of deep UV to free radicals such as $H^{\bullet}$, $CO^{\bullet}$, $CO_2^{\bullet}$, $R^{\bullet}$ and hydrated electrons [14, 18, 19]. These radicals can interact with the elements of interest to form volatile compounds. The identity of radicals and generated volatile compounds strongly depend on the LMWOA used, i.e., hydrides or carbonyls are generated from the formic acid medium, methyl and ethyl derivatives from acetic and propionic acid media, respectively [18]. UV-PVG has been used to generate volatile compounds of approximately 30 elements that in addition to Te include other conventional hydride forming elements, transition metals and even non-metals [14, 21–36].

The first successful UV-PVG of Te was demonstrated by Guo et al. [14] using a batch style UV reactor. This was followed by more in-depth studies [21, 22, 24] using various flow arrangements of the photoreactors and LMWOA as reaction media (formic acid or mixture of formic and acetic acid). The overall generation efficiency seemed to be rather low, hence, nano-TiO_2 [37] and transition metal ions as sensitizers (namely Fe(II)/(III) [37, 38], Co(II) [32], Mn(II) [38] and V(IV)/V(V) [39]) added to the reaction media have been employed to substantially enhance the overall generation efficiency of UV-PVG of Te(IV). The addition of photocatalysts (TiO_2 [37] or V(V) [39]) allowed efficient UV-PVG also from Te(VI) and resulted in equal generation efficiency and thus sensitivity as for Te(IV). The majority of those studies relied on a flow-through quartz photoreactor that provided high radiation intensity as well as ready access to 254 nm and 185 nm emission lines of Hg. The exception is our recent work [38] in which we employed a simple reactor consisting of a PTFE reaction coil (access to only 254 nm line) wrapped around a low-pressure Hg tube lamp and Mn(II) and Fe(II) ions as sensitizers for UV-PVG of Te(IV). The developed analytical methodology was then applied to non-chromatographic oxidation state speciation analysis of Te that was based on an off-line pre-reduction of Te(VI) to Te(IV) in 6 mol dm^{-3} HCl at 95 °C prior to UV-PVG.

A typical experimental setup of the generators lies in a single channel through which the reaction medium is carried to the photoreactor where the sample is irradiated. The carrier gas (exclusively Ar), by which the generated volatile compound is stripped to the gas phase, is introduced downstream of the photoreactor, thus permitting sufficient time for irradiation of the sample. Only few papers described introduction of a carrier gas upstream of the photoreactor [15, 21, 31, 40–45]. Such setup inherently limits the irradiation time to seconds and thus possibly reduces the production of reducing radicals to those that are formed fast but, at the same time, it may reduce the risk of decomposition of unstable volatile compounds under UV irradiation.

In this work, we focused on optimization of UV-PVG of Te(IV) in a continuous flow mode using the PTFE coiled photoreactor where the flow of a carrier gas was admitted upstream of the photoreactor (hereafter denoted as "thin-film photoreactor"). UV-PVG was studied using only Te(IV) standards in the absence of any sensitizers or photocatalysts reported previously for efficient UV-PVG also from Te(VI) [37, 39]. The differences in performance (figures of merit, interferences and overall generation efficiency) and optimal conditions compared to previous publications employing the standard photoreactor setups are discussed.

Results and discussion

A crucial part of this work was the optimization of the experimental conditions for UV-PVG of Te(IV) using a thin-film photoreactor to achieve maximum sensitivity. The critical experimental parameters were concentration and composition of the reaction medium and flow rate of the carrier gas. We also optimized atomization conditions in the externally heated quartz tube atomizer (EHT) including the atomization temperature and addition of H_2. This was followed by

an examination of potential interferences from several transition metals, metalloids and inorganic anions. Analytical characteristics were evaluated at chosen optimal conditions using both a line source AAS (LS-AAS) and high-resolution continuum source AAS (HR-CS-AAS). Moreover, we also determined the overall generation efficiency. The results are discussed with respect to those obtained recently in a very similar UV-PVG apparatus but with introduction of carrier gas downstream of the photoreactor [38] (hereafter denoted as "standard flow photoreactor").

Optimization of reaction medium

UV-PVG of elements is typically carried out in the presence of LMWOA producing suitable reducing radicals (see Introduction). Concentration of LMWOA is crucial, because on one hand, lower concentration of acid does not produce enough radicals to convert the analyte to volatile compounds, and on the other hand, excessive concentration of acid may lead to low penetration of the UV radiation into the sample or to competitive formation of other organic compounds in the reaction medium due to radical recombination, thereby reducing the generation efficiency of the volatile compounds. Since Te can form volatile hydride as well as alkylated compounds, we tested the effect of formic, acetic and propionic acid on UV-PVG of Te(IV) using the thin-film photoreactor supplied with 125 cm^3 min^{-1} carrier $Ar_{(upstream)}$. Each acid was tested individually over a range of concentrations 0.5–5.0 mol dm^{-3} (Fig. 1). Acetic acid was found the most suitable acid with maximum response at 4 mol dm^{-3}, followed by propionic acid, wherein a plateau of maximum AAS response was obtained in the range

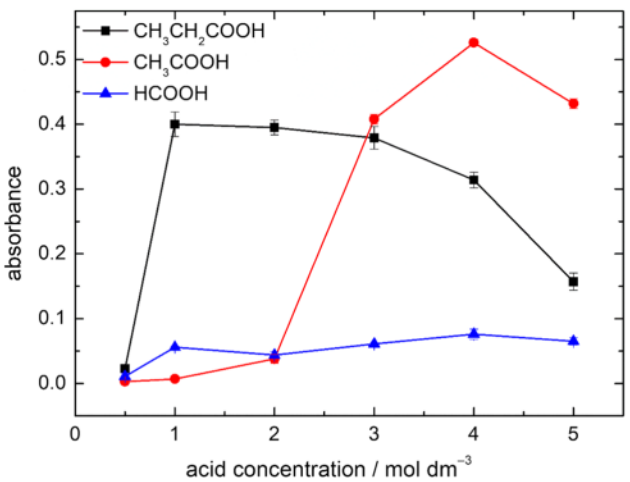

Fig. 1 Effect of low molecular weight organic acids used for UV-photochemical vapor generation of Te(IV); conditions: 1.0 mg dm^{-3} Te(IV), 2.5 cm^3 min^{-1} sample flow rate, 125 cm^3 min^{-1} carrier $Ar_{(upstream)}$ flow rate, 12 cm^3 min^{-1} hydrogen flow rate, 900 °C atomizer temperature

1–3 mol dm^{-3}. Formic acid gave four or five times lower signals at maximum (4 mol dm^{-3}) than propionic or acetic acid despite being shown previously that the absorption of 254 nm is more efficient in formic than in acetic acid [38]. We also tried various mixtures of LMWOAs but no improvement was observed. The 4.0 mol dm^{-3} acetic acid medium was thus used for subsequent experiments.

The influence of a sample flow rate was investigated in the range 2–4 cm^3 min^{-1}. The maximum response was obtained at 2.8 cm^3 min^{-1}, so this value was chosen as an optimum for next experiments.

Influence of the carrier gas flow rate

The carrier gas is important for the processes of gas–liquid separation and transport of the volatile compounds to the EHT. It also influences atomization in the EHT, because excessive flow rates cause dilution of free atoms resulting in lower sensitivity. As noted in the Introduction section, a typical point of introduction of carrier gas is downstream of the photoreactor. It is either mixed in a T-piece with the stream of the irradiated reaction medium exiting the photoreactor or added to the gas–liquid separator (GLS), e.g., through a frit. The alternative arrangement where the carrier gas is introduced to the generator upstream of the photoreactor was found by some authors more suitable for UV-PVG [15, 21, 31, 40–45] bringing, most probably, the benefits of fast separation of generated volatile species from the liquid media. It, however, inevitably leads to much shorter irradiation times that are almost solely driven by the flow of carrier $Ar_{(upstream)}$.

Using 4 mol dm^{-3} acetic acid as the reaction medium, the carrier Ar was optimized by independently varying two Ar flows introduced at two points—upstream and downstream of the photoreactor (Fig. 2). The former one especially affects the irradiation time in the photoreactor, gas–liquid separation as well as transport of volatile compounds to the atomizer. The latter one finely customizes the optimum flow rate suitable for atomization in the EHT and can reduce transport losses in the gas phase.

It is evident that AAS response increased with increasing flow rate of carrier $Ar_{(upstream)}$ up to 250 cm^3 min^{-1}. This flow seems to be relatively high, in comparison to UV-PVG of Se(IV) [40–42], which might be explained by lower stability of generated volatile compounds and/or difficult release from the liquid medium. Additional flow of carrier Ar introduced downstream of the photoreactor had lower effect, but even so, sensitivity further increased with additional $Ar_{(downstream)}$ of 50 cm^3 min^{-1}. Further increasing of carrier Ar flow rates likely diluted free atoms in the observed volume of the EHT. Therefore, we chose a combined introduction of carrier Ar to the generator using 250 cm^3 min^{-1} of $Ar_{(upstream)}$ and 50 cm^3 min^{-1} of $Ar_{(downstream)}$.

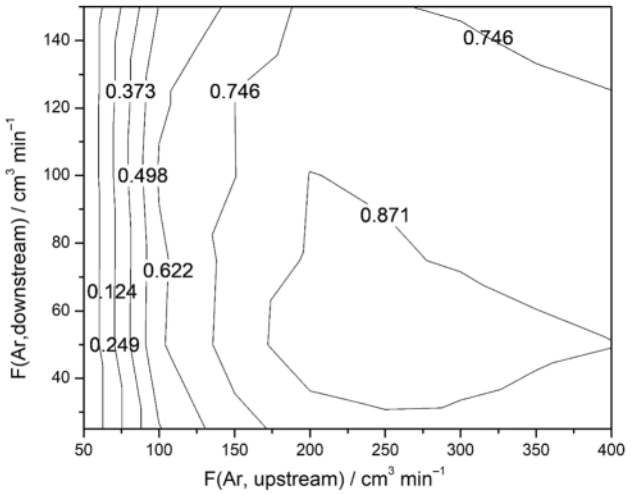

Fig. 2 Dependence of AAS response on carrier Ar with simultaneous introduction upstream and downstream of the photoreactor; conditions: 1.0 mg dm^{-3} Te(IV) in 4.0 mol dm^{-3} acetic acid, 2.8 cm^3 min^{-1} sample flow rate, 12 cm^3 min^{-1} hydrogen flow rate, 900 °C atomizer temperature

Optimization of the atomization conditions

The presence of H_2 and increased temperature is required to produce hydrogen radicals that are responsible for atomization of volatile compounds in the EHT [46]. In the case of UV-PVG, it is necessary to add some amount of H_2 to the carrier gas, because its production during UV-PVG is not sufficient as opposed to HG in which necessary amount of H_2 is delivered from decomposition of $NaBH_4$. Our apparatus utilized a combined GLS and atomizer device (in one piece) minimizing transport losses of the volatile compounds. The GLS part was equipped with a special inlet for introduction of H_2 placed next to the inlet for introduction of a mixture of carrier Ar and reaction medium (see Experimental). The flow rate of H_2 was optimized in the range 0–35 cm^3 min^{-1}. The signal sharply increased up to 12 cm^3 min^{-1} and then levelled off, the values over 20 cm^3 min^{-1} did not change the AAS response. Absolutely no AAS response was observed without added H_2 proving that H_2 was not generated in the photoreactor or that its production was insufficient for atomization. Temperature of the EHT was optimized in the range 700–1025 °C. As expected, temperatures higher than 900 °C were necessary for efficient atomization of volatile compounds, thus proving that the tellurium species were molecular in nature (most probably dimethyl telluride). The chosen optimum conditions for UV-PVG in the thin-film photoreactor and atomization in the EHT are summarized in Table 1.

Table 1 Optimum experimental conditions for UV-photochemical vapor generation of Te(IV) in the thin-film photoreactor and atomization in the externally heated quartz tube atomizer

Parameter	Value
Acetic acid concentration/mol dm^{-3}	4.0
Sample flow rate/cm^3 min^{-1}	2.8
Carrier $Ar_{(upstream)}$ flow rate/cm^3 min^{-1}	250
Carrier $Ar_{(downstream)}$ flow rate/cm^3 min^{-1}	50
Irradiated volume/cm^3	2.4
Flow rate of H_2/cm^3 min^{-1}	20
Atomizer temperature/°C	950

Interferences

Another important aspect of an analytical method is its resistance to interferences. UV-PVG is generally liable to interferences from other hydride forming elements, transition metals, radical scavengers, inorganic acids and their salts [18, 45]. In addition, the presence of some transition metals was shown to significantly enhance overall generation efficiency of numerous analytes [47]. These effects are likely to be influenced by the fast stripping of volatile compounds too, therefore, we focused also on the impact of such interferences (or potential sensitizers).

The effects of three typical hydride forming elements (As(III), Se(IV) and Pb(II)) and six transition metals (Fe(II), Cu(II), Ni(II), Co(II), Cd(II) and Mn(II)) were examined (Table 2) in the concentration range 0.5–50 mg dm^{-3} or 0.5–500 mg dm^{-3} in the case of Mn(II). The transition elements and their concentrations were selected to complement the results obtained with the standard flow photoreactor [38]. The thin-film photoreactor was operated under the conditions summarized in Table 1. The most significant interference was evident for Cd(II), which probably forms CdTe. Tellurium is known to form CdTe with cadmium ions in aqueous solution [48, 49] and analogous formation of CdSe was already observed during PVG of Se(IV) [50]. Contrary to the positive effect of formation CdSe on UV-PVG of Se species [50], the formation of CdTe had detrimental effect in our work. Nevertheless, it very well agrees with our previous work in which UV-PVG was conducted in the standard flow photoreactor [38]. Quite serious interference was also evident for Se(IV) ions already at 5 mg dm^{-3} level. The system was quite tolerant to the presence of Cu(II), which was found to cause serious interference in the previous papers on UV-PVG of Te(IV) sensitized with transition metals [32, 37, 38]. Conversely to the works by He et al. [37] and Zeng et al. [32] who used a mixture of acetic and formic acid and Fe(II)/Fe(III) and Co(II) as sensitizers for UV-PVG of Te(IV) we observed no or only

Table 2 Influence of various co-existing ions on Te(IV) determination (0.5 mg dm^{-3})

Interferent concentration/mg dm^{-3}	Recoveries[a] in the presence of interferent / %								
	As(III)	Se(IV)	Pb(II)	Fe(II)	Cu(II)	Ni(II)	Co(II)	Cd(II)	Mn(II)
0.5	102	80	52	91	87	108	85	4	102
5	94	5	22	110	58	105	80	0	109
50	0	0	0	32	0	17	33	0	125
250	_[b]	_[b]	_[b]	_[b]	_[b]	_[b]	_[b]	_[b]	153
500	_[b]	_[b]	_[b]	_[b]	_[b]	_[b]	_[b]	_[b]	149

[a]Relative combined SD (combined SD/recovery) was < 2% for all recovery values

[b]Not determined

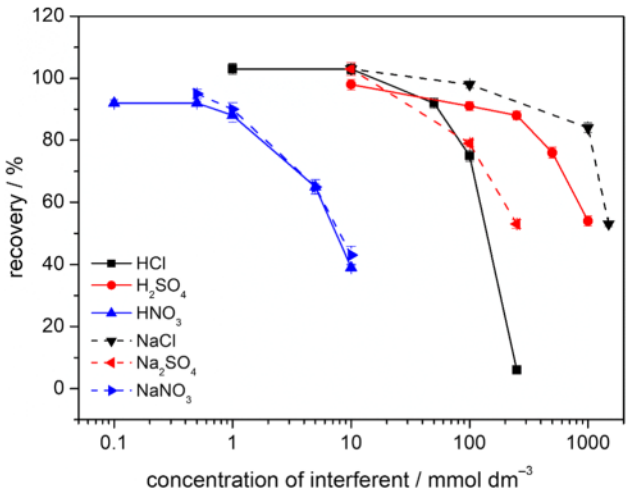

Fig. 3 Relative effects of added interferents on AAS response of 0.5 mg dm^{-3} Te(IV); conditions: 4 mol dm^{-3} acetic acid, sample flow rate 2.8 cm^3 min^{-1}, 250 cm^3 min^{-1} carrier $Ar_{(upstream)}$ flow rate, 50 cm^3 min^{-1} carrier $Ar_{(downstream)}$ flow rate, 20 cm^3 min^{-1} hydrogen flow rate, 950 °C atomizer temperature

little positive effects from Co(II) or Fe(II) and Ni(II) ions (Table 2), which rules out their use as sensitizers in our system. The only exception was Mn(II) that increased the AAS response by around 50% at 250 and 500 mg dm^{-3} in a similar way as when using the standard flow photoreactor [38].

Interferences caused by inorganic anions (NO_3^-, SO_4^{2-}, Cl^-) added in the form of acids or sodium salts were also investigated (Fig. 3). The presence of NO_3^- was found the most serious interferent wherein a serious decrease in AAS response (by around 35%) was found at 5 mmol dm^{-3} for both HNO_3 and $NaNO_3$. The UV-PVG system was much more tolerant to the presence of other inorganic anions, because a significant interference (> 10% decrease) was identified at 100 mmol dm^{-3} HCl, 100 mmol dm^{-3} Na_2SO_4, 250 mmol dm^{-3} H_2SO_4, and 1000 mmol dm^{-3} NaCl. In comparison to our standard flow photoreactor [38], it seems that the thin-film system is similarly or only slightly less tolerant to all tested anions.

Figures of merit and generation efficiency

The figures of merit were evaluated using both LS-AAS and HR-CS-AAS as detectors at the optimal conditions for the thin-film photoreactor. The LOD obtained with LS-AAS was 5.6 µg dm^{-3} and 0.85 µg dm^{-3} was achieved with HR-CS-AAS using 5 pixels of the CCD detector for evaluation. The repeatability at 250 µg dm^{-3} was in the range 1.1–1.2% (n = 10) and the linear dynamic range of calibrations was 19–1000 µg dm^{-3} and 3–1000 µg dm^{-3} for LS-AAS and HR-CS-AAS, respectively.

The LOD obtained with HR-CS-AAS is about four times lower than that achieved with the same detector using the standard photoreactor for UV-PVG of Te(IV) in the presence of Mn(II) and Fe(II) ions as sensitizers [38]. Furthermore, the repeatability was about twice better in this work. Nevertheless, it should be noted that a different way of sample introduction (flow injection mode) and atomizer (miniature diffusion flame atomizer) were utilized in the previous work [38].

Overall generation efficiency was determined according to our previously published procedure [29–31, 33, 51, 52] using ICP-MS. The comparison of sensitivities obtained with UV-PVG in the thin-film photoreactor and solution nebulization coupled to ICP-MS was carried out using a flow injection for sample delivery (see Experimental section for details). The overall generation efficiency reached 7.7 ± 0.2%.

Discussion

The achieved results can now be discussed and compared in the light of our earlier work with the standard flow photoreactor (the same length and dimensions of the PTFE coiled photoreactor and source of UV radiation) in which the carrier Ar was introduced downstream of the photoreactor [38]. A special continuous flow arrangement where the flow of carrier Ar was admitted upstream of the photoreactor can be characterized as a true "thin-film" setup. The flow rate of carrier gas is too high to form individual bubbles (segments)

in the reaction medium. Correspondingly, observation of the liquid flowing through the reactor (with the lamp turned off) did not show any segmentation or pulsing. This is further supported by stable steady-state AAS signals and the UV-PVG process can be characterized by excellent repeatability (around 1%). The carrier gas reproducibly forms a channel in the middle of the PTFE capillary forcing the liquid to form a thin film along the walls of the PTFE capillary. This film enables effective penetration of UV radiation into the whole depth of the liquid and permits an immediate release of generated volatile compounds of Te into the carrier gas. The formation of individual channels for gas and liquid film is supported by a visual observation of the movement of a zone of liquid (with lamp turned off) after its introduction into the "dry" system.

This also allowed to estimate the irradiation time to 6.8 s. This is significantly longer than 0.57 s, which could be derived from the internal volume of the PTFE coil (2.4 cm^3) and the sum of carrier gas (250 cm^3 min^{-1}) and reaction medium (2.8 cm^3 min^{-1}) flow rates. However, it is significantly shorter than the irradiation time for the standard flow photoreactor when the sample is propelled only by the flow of liquid (51 s at 2.8 cm^3 min^{-1}). It should be noted that optimum irradiation time in the range 21–36 s was found in the standard flow photoreactor previously [38].

The differences in the thickness of the irradiated liquid medium, irradiation time and gas–liquid separation process are the reasons for completely different optimum composition of the reaction media for UV-PVG of Te(IV) conducted in the thin-film and the standard flow photoreactors [38]. While only 4 mol dm^{-3} acetic acid as the reaction medium was suitable for the thin-film photoreactor (Fig. 1), no formation of volatile species was observed in the range 1–4 mol dm^{-3} of acetic acid using the standard flow photoreactor and only negligible responses were recorded at 6–8 mol dm^{-3}. For efficient UV-PVG in the standard photoreactor, the reaction medium consisting of a mixture of 5 mol dm^{-3} acetic acid and 3.5 mol dm^{-3} formic acid was necessary [38]. Conversely, this composition of the reaction medium provided only 4% AAS response in the thin-film setup in comparison to the response obtained from 4 mol dm^{-3} acetic acid. Another interesting point is the ineffectiveness of the same concentrations of Fe(II) ions as sensitizer in the thin-film setup in comparison to the standard flow photoreactor while Mn(II) ions worked similarly [38].

It may appear from the determined value of the overall generation efficiency (around 8%) that the UV-PVG process is not efficient enough and is rather marginal in comparison to the efficiency of 50% achieved recently in the standard flow photoreactor [38]. However, a proper comparison should be made under similar conditions considering also the effects of metal(s) sensitizers and the carrier Ar flows admissible for AAS measurements. First, the value of overall generation efficiency for the standard flow system without the use of Mn(II) and Fe(II) ions sensitizers could be estimated 2.75-fold lower reaching thus approximately 18% [38]. Similarly, addition of Mn(II) ions to 4 mol dm^{-3} acetic acid improves the efficiency of the thin-film photoreactor, as evident in Table 2, by a factor of 1.53 to almost 12%. Nevertheless, the use of sensitizers (Mn(II) or combination of Mn(II) and Fe(II)) is not suitable for long-term measurements with the continuous flow mode irrespective of the generator used. On-line loading of Mn(II) (and also Fe(II)) causes deposition of reduced metals and may decrease transmittance of the UV radiation through the inner walls of the photoreactor, which is reflected on slowly decreasing AAS sensitivity. Second, in the view of AAS measurements with the EHT, the effect of total carrier Ar should be also considered. A very high influence of carrier Ar on the release of volatile Te compounds was identified in the standard photoreactor [38] when the maximum overall generation efficiency and ICP-MS sensitivity was achieved at 800 cm^3 min^{-1} of carrier Ar, which was 1.6-fold higher than at 250 cm^3 min^{-1}. However, such a high flow rate is not compatible with AAS measurements due to pronounced dilution of free atoms in the observed volume of the atomizer. It would, therefore, make sense to adjust the theoretical efficiency (without sensitizers) to the flow rate of 300 cm^3 min^{-1} by a factor of 1.5 to value of 12%, which is not so far from 8% achieved in this work. To conclude this discussion, after subtracting the effect of different experimental conditions, the performance of both the systems for the combination with AAS is comparable.

Conclusions

UV-PVG was investigated in a special continuous flow arrangement where the carrier gas was admitted upstream of the photoreactor to create a thin film of the reaction medium facilitating effective UV irradiation. Surprisingly, this led to different optimum reaction conditions then those found suitable for the standard generator, i.e., supplied with the carrier gas downstream of the photoreactor.

This is definitely interesting from the mechanistic point of view and may explain inconsistencies and conflicting conclusions drawn about optimum conditions for UV-PVG of various analytes. Although the overall generation efficiency is lower in the thin-film photoreactor, in combination with the high liquid sample flow rate through the system, still a high analyte flux in the form of volatile compounds to the atomizer and detector can be reached, which may overcome other techniques of sample introduction for AAS in terms of LOD. In addition, the analyte delay in the photoreactor is really short, which increases sample throughput and enables automatization.

Experimental

Instrumentation

A scheme of the apparatus for UV-PVG, atomization and AAS detection is shown in Fig. 4. Solutions were continuously pumped with a peristaltic pump (Ismatec, Cole-Parmer, Germany) using Tygon© tubing (1.42 mm i.d., Ismatec, Germany). All other tubing was made of PTFE (1.58 mm o.d., 0.8 mm i.d., Sigma-Aldrich, USA). Tellurium volatile compounds were generated in the photoreactor made of a low-pressure mercury UV bench lamp (20 W, dimensions 610 × 35 mm, Ushio, Japan) which was tightly wrapped with the PTFE reaction coil (1.58 mm o.d., 0.8 mm i.d., 480 cm long, Sigma-Aldrich, USA). The PTFE photoreactor was placed in a power supply with mirror walls and covered with an aluminium foil to protect the operator from UV radiation. Carrier gas (Ar) facilitated release of volatile compounds from the liquid phase and transported them to an externally heated T-shaped quartz tube atomizer (EHT, RMI, Czech Republic) for detection. It was introduced to the apparatus upstream and downstream of the UV-photoreactor using two PTFE T-pieces. The flow rates of carrier $Ar_{(upstream)}$ and $Ar_{(downstream)}$ were controlled by mass-flow controllers (Cole-Palmer, USA). A gas–liquid separator (GLS) with a forced outlet served for separation of volatile compounds from the liquid phase that was removed by the peristaltic pump. The outlet of the GLS was directly connected to the inlet arm of the EHT (in a single piece) to minimize transport losses in the gas phase [43]. The inner volume of the GLS was 7.0 cm^3 (not including the inlet arm of the EHT). The GLS was equipped with a special inlet for hydrogen supply (controlled by a mass-flow controller) to support atomization in the EHT [43].

AAS measurements were made using either a line source spectrometer AA Solaar 939 (LS-AAS, Unicam, UK) equipped with a tellurium hollow cathode lamp (Heraeus, Germany) and operated at 12 mA or a high-resolution continuum source spectrometer ContrAA 300 (HR-CS-AAS, Analytik Jena, Germany) equipped with a Xe short-arc lamp operated in a hot-spot mode. The detection with the LS-AAS instrument was carried out at 214.3 nm with 0.5 nm slit width while the detection with the HR-CS-AAS instrument was carried out using 5 pixels of the charge coupled device (CCD) array as a detector when the central pixel was set at 214.281 nm. The spectral resolution corresponded to 1.5 pm/pixel. LS-AAS was used as the detector for all experiments while HR-CS-AAS was used only for determination of analytical characteristics.

ICP-MS (Agilent 7700x) equipped with a MicroMist nebulizer was used for determination of the overall generation efficiency. UV-PVG was connected to the ICP-MS via the dilution gas inlet (high matrix introduction system) in the same way as described in Ref. [51].

Reagents and samples

Deionized water prepared by a MilliQplus system (18.2 MΩ cm; Millipore, USA) was used for the preparation of all solutions. The solution of 100 mg dm^{-3} of Te(IV) was prepared by dissolving 17.36 mg of sodium tellurite (> 99%, Sigma-Aldrich, USA) in 100 cm^3 deionized water. Formic acid (≥ 98%, Merck, Germany), acetic acid (≥ 99.5%, Sigma-Aldrich, USA) and propionic acid (≥ 99.5%, Fluka, Germany) were used for preparation of the reaction media for UV-PVG and their solutions were prepared daily. Argon (99.998%, Linde Gas, Czech Republic) and hydrogen

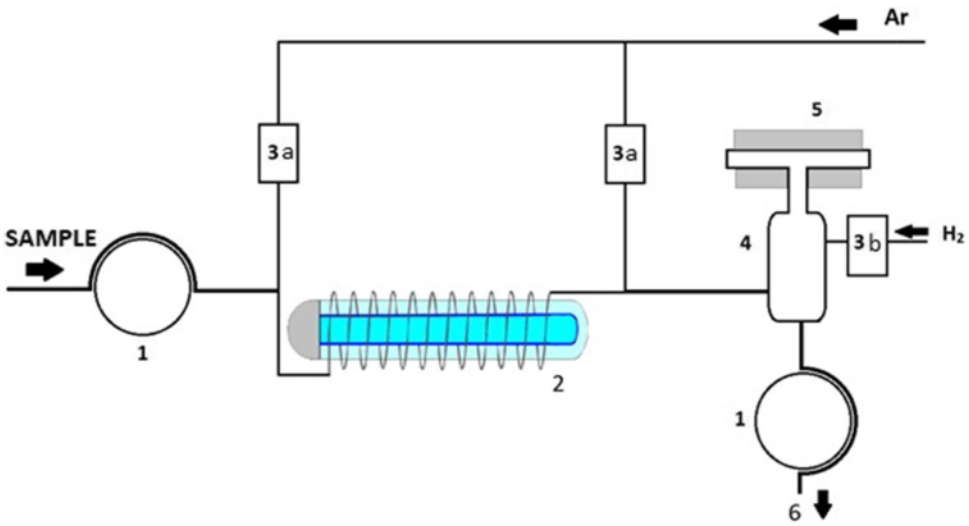

Fig. 4 Experimental arrangement of the UV-photochemical vapor generator coupled to the combined gas–liquid separator and atomizer device, numbers in the diagram represent peristaltic pumps (1), photoreactor (2), mass-flow controllers for Ar (3a) and H_2 (3b), gas–liquid separator (4), externally heated T-shaped quartz tube atomizer (5) and waste outlet (6)

(99.90%, Linde Gas, Czech Republic) were used during all experiments. Stock solutions of elements tested during the interference study were prepared by dissolving the following compounds in deionized water: arsenous acid (p.a., ≥ 99.99%, Sigma-Aldrich, USA), sodium selenite pentahydrate (p.a., ≥ 99.0%, Fluka, Germany), lead(II) acetate trihydrate (p.a., ≥ 99.99%, Sigma-Aldrich, USA), iron(II) sulfate heptahydrate (p.a., Lachema, Czech Republic), cobalt(II) acetate tetrahydrate (p.a., Lach-Ner, Czech Republic), copper(II) acetate monohydrate (p.a., ≥ 99.99%, Sigma-Aldrich, USA), cadmium(II) acetate dihydrate (p.a., Lach-Ner, Czech Republic), nickel(II) sulfate heptahydrate (p.a., ≥ 99.999%, Sigma-Aldrich, USA), manganese(II) acetate tetrahydrate (p.a., Sigma-Aldrich, USA). Other chemicals were sourced as follows: nitric acid (semiconductor grade, 65%) from Honeywell (USA); hydrochloric acid (p.a., 37%), sodium nitrate and sodium sulfate from Merck (Germany); sulfuric acid (p.a., 98%) from Lach-Ner (Czech Republic); and sodium chloride from Lachema (Czech Republic).

Procedure

The blank containing LMWOA in deionized water was continuously pumped by the peristaltic pump into the PTFE coiled UV-photoreactor. After the signal was stabilized on the baseline, the blank flow was switched to the flow of sample prepared in LMWOA. With the exception of the overall generation efficiency, all the measurements were carried out in the continuous flow mode. The new measurement was initiated after the signal had stabilized at the baseline.

Determination of overall generation efficiency

The overall generation efficiency was determined by comparison with nebulization efficiency described previously [29–31, 33, 52]. The ICP-MS was tuned while running the UV-PVG. Tellurium solutions (0, 2.5, 10 and 25 μg dm^{-3}) prepared in 4 mol dm^{-3} acetic acid were sequentially analysed using UV-PVG, while nebulizing internal standards and 2% (m/v) HNO_3. Succeeding that, tellurium solutions (0, 5, 20 and 50 μg dm^{-3}) prepared in 2% (m/v) HNO_3 were nebulized along with internal standards while UV-PVG reaction was running with blank solution at the same experimental conditions. The detection was carried out in a pulse mode for ^{125}Te and ^{103}Rh (internal standard) isotopes using no gas in the reaction/collision cell. The resulting time dependent signals were treated in MS Excel software. Overall UV-PVG efficiency is defined as the fraction of analyte converted to a volatile compound, released from the liquid phase and transported by a carrier gas to the ICP-MS. In our calculation, the overall generation efficiency ε_{PVG} is the ratio of the sensitivities for UV-PVG a_{PVG} and nebulization a_{neb} multiplied by nebulization efficiency ε_{neb} (Eq. (1)). The sample volume was the same (0.5 cm^3) for both ways of sample introduction.

$$\varepsilon_{PVG} = \left(a_{PVG}/a_{neb}\right) \cdot \varepsilon_{neb}. \quad (1)$$

Nebulization efficiency was determined by a modified waste collection method, Ref. [29–31, 33, 51, 52] for details.

Conventions

With the exception of determination of overall generation efficiency using ICP-MS, steady-state absorbance value corrected for the baseline was employed as a measure of analytical response. Each result is presented as the average of at least three replicates with an uncertainty given as ± one standard deviation (SD) or combined SD where results are relative (e.g., interference study).

Repeatability was calculated as a relative standard deviation (RSD) of 10 consecutive determinations of a 250 μg dm^{-3} Te(IV) standard. Limit of detection (LOD) was calculated from three SD of ten measurements of the solution with concentration of 20 μg dm^{-3} Te(IV). The linear dynamic range is here defined as the section of a calibration curve, for which the coefficient of determination is better or equal to 0.98. The low end of the linear dynamic range equals to limit of quantification.

Acknowledgements The authors thank Charles University for financial support. This research was carried out within the framework of Specific University Research (Project SVV 260560) and with grant support of the Grant Agency of Charles University (Project GA UK 516119) and the Czech Academy of Sciences (Institutional support RVO: 68081715).

References

1. Ogra Y (2017) Metallomics 9:435
2. Najimi S, Shakibaie M, Jafari E, Ameri A, Rahimi N, Forootanfar H, Yazdanpanah M, Rahimi HR (2017) Regul Toxicol Pharmacol 90:222
3. Ba LA, Döring M, Jamier V, Jacob C (2010) Org Biomol Chem 8:4203
4. Filella M, Reimann C, Biver M, Rodushkin I, Rodushkina K (2019) Environ Chem 16:215
5. Cobelo-García A, Filella M, Croot P, Frazzoli C, Du Laing G, Ospina-Alvarez N, Rauch S, Salaun P, Schäfer J, Zimmermann S (2015) Environ Sci Pollut Res 22:15188
6. Cava-Montesinos P, Cervera LM, Pastor A, de la Guardia M (2004) Talanta 62:173
7. Cava-Montesinos P, Cervera LM, Pastor A, de la Guardia M (2003) Anal Chim Acta 481:291
8. Zhang N, Fu N, Fang ZT, Feng YH, Ke L (2011) Food Chem 124:1185
9. Pedro J, Stripekis J, Bonivardi A, Tudino M (2008) Spectrochim Acta Part B 63:86
10. Yildirim E, Akay P, Arslan Y, Bakirdere S, Ataman OY (2012) Talanta 102:59
11. Filella M, Rodushkin I (2018) Spectrochim Acta Part B 141:80

12. Tan Q, Pan Y, Liu L, Shu SB, Liu Y (2019) Microchem J 144:495
13. Dědina J, Tsalev DL (1996) Hydride generation atomic absorption spectrometry. Wiley, Chichester
14. Guo XM, Sturgeon RE, Mester Z, Gardner GJ (2004) Anal Chem 76:2401
15. Linhart O, Kolorosová-Mrázová A, Kratzer J, Hraníček J, Červený V (2019) Anal Lett 52:613
16. Luo J, Hu ZH, Xu FJ, Geng DX, Tang XL (2022) Microchem J 174:107053
17. Sun YC, Chang YC, Su CK (2006) Anal Chem 78:2640
18. Leonori D, Sturgeon RE (2019) J Anal At Spectrom 34:636
19. Sturgeon RE (2017) J Anal At Spectrom 32:2319
20. Rybínová M, Červený V, Hraníček J, Rychlovský P (2015) Chem Listy 109:930
21. Romanovskiy K, Bolshov M, Münz A, Temerdashev Z, Burylin M, Sirota K (2018) Talanta 187:370
22. Zheng CB, Ma Q, Wu L, Hou XD, Sturgeon RE (2010) Microchem J 95:32
23. Sturgeon RE, Pagliano E (2020) J Anal At Spectrom 35:1720
24. de Quadros DPC, Borges DLG (2014) Microchem J 116:244
25. Hu J, Sturgeon RE, Nadeau K, Hou XD, Zheng CB, Yang L (2018) Anal Chem 90:4112
26. de Oliveira RM, Borges DLG (2018) J Anal At Spectrom 33:1700
27. Zhou J, Deng D, Su YY, Lv Y (2019) Microchem J 146:359
28. Wang YL, Lin LL, Liu JX, Mao XF, Wang JH, Qin DY (2016) Analyst 141:1530
29. Vyhnanovský J, Yildiz D, Štádlerová B, Musil S (2021) Microchem J 164:105997
30. Vyhnanovský J, Sturgeon RE, Musil S (2019) Anal Chem 91:13306
31. Nováková E, Horová K, Červený V, Hraníček J, Musil S (2020) J Anal At Spectrom 35:1380
32. Zeng W, Hu J, Chen HJ, Zou ZR, Hou XD, Jiang XM (2020) J Anal At Spectrom 35:1405
33. Musil S, Vyhnanovský J, Sturgeon RE (2021) Anal Chem 93:16543
34. Gao Y, Xu M, Sturgeon RE, Mester Z, Shi ZM, Galea R, Saull P, Yang L (2015) Anal Chem 87:4495
35. Šoukal J, Sturgeon RE, Musil S (2018) Anal Chem 90:11688
36. Grinberg P, Sturgeon RE (2009) J Anal At Spectrom 24:508
37. He HY, Peng XH, Yu Y, Shi ZM, Xu M, Ni S, Gao Y (2018) Anal Chem 90:5737
38. Jeníková E, Nováková E, Hraníček J, Musil S (2022) Anal Chim Acta 1201:339634
39. Dong L, Chen HJ, Ning YY, He YW, Yu Y, Gao Y (2022) Anal Chem 94:4770
40. Rybínová M, Červený V, Hraníček J, Rychlovský P (2016) Microchem J 124:584
41. Rybínová M, Červený V, Rychlovský P (2015) J Anal At Spectrom 30:1752
42. Rybínová M, Musil S, Červený V, Vobecký M, Rychlovský P (2016) Spectrochim Acta Part B 123:134
43. Linhart O, Smolejová J, Červený V, Hraníček J, Nováková E, Resslerová T, Rychlovský P (2016) Monatsh Chem 147:1447
44. Nováková E, Linhart O, Červený V, Rychlovský P, Hraníček J (2017) Spectrochim Acta Part B 134:98
45. Nováková E, Rybínová M, Hraníček J, Rychlovský P, Červený V (2018) J Anal At Spectrom 33:118
46. Dědina J, Welz B (1992) J Anal At Spectrom 7:307
47. Zhen YF, Chen HJ, Zhang M, Hu J, Hou XD (2021) Appl Spectrosc Rev 57:318
48. Li L, Qian HF, Fang NH, Ren JC (2006) J Lumin 116:59
49. Gao MY, Kirstein S, Möhwald H, Rogach AL, Kornowski A, Eychmüller A, Weller H (1998) J Phys Chem B 102:8360
50. Xu FJ, Zou ZR, He J, Li MT, Xu KL, Hou XD (2018) Chem Commun 54:4874
51. Bufková K, Musil S, Kratzer J, Dvořák P, Mrkvičková M, Voráč J, Dědina J (2020) Spectrochim Acta Part B 171:105947
52. Sagapova L, Musil S, Kodríková B, Svoboda M, Kratzer J (2021) Anal Chim Acta 1168:338601

analytical chemistry

pubs.acs.org/ac Article

Highly Efficient Photochemical Vapor Generation for Sensitive Determination of Iridium by Inductively Coupled Plasma Mass Spectrometry

Stanislav Musil,* Eva Jeníková, Jaromír Vyhnanovský, and Ralph E. Sturgeon

Cite This: https://doi.org/10.1021/acs.analchem.2c04660 Read Online

ACCESS | Metrics & More | Article Recommendations | Supporting Information

ABSTRACT: Herein, we describe the highly efficient photochemical vapor generation (PVG) of a volatile species of Ir (presumably iridium tetracarbonyl hydride) for subsequent detection by inductively coupled plasma mass spectrometry (ICPMS). A thin-film flow-through photoreactor, operated in flow injection mode, provided high efficiency following optimization of identified key PVG parameters, notably, irradiation time, pH of the reaction medium, and the presence of metal sensitizers. For routine use and analytical application, PVG conditions comprising 4 M formic acid as the reaction medium, the presence of 10 mg L^{-1} Co^{2+} and 25 mg L^{-1} Cd^{2+} as added sensitizers, and an irradiation time of 29 s were chosen. An almost 90% overall PVG efficiency for both Ir^{3+} and Ir^{4+} oxidation states was accompanied by excellent repeatability of 1.0% (n = 15) of the peak area response from a 50 ng L^{-1} Ir standard. Limits of detection ranged from 3 to 6 pg L^{-1} (1.5−3 fg absolute), dependent on use of the ICPMS reaction/collision cell. Interferences from several transition metals and metalloids as well as inorganic acids and their anions were investigated, and outstanding tolerance toward chloride was found. Accuracy of the developed methodology was verified by analysis of NIST SRM 2556 (Used Auto Catalyst) following peroxide fusion for sample preparation. Practical application was further demonstrated by the direct analysis of spring water, river water, lake water, and two seawater samples with around 100% spike recovery and no sample preparation except the addition of formic acid and the sensitizers.

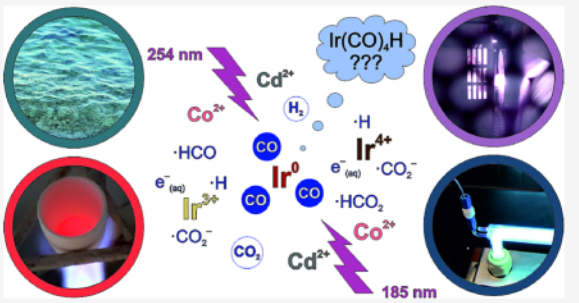

INTRODUCTION

Iridium belongs to the platinum group metals (PGMs) and is one of the rarest elements on Earth. For example, the concentration of dissolved Ir in seawater was reported to be in the range 0.1−10 pg L^{-1}.[1,2] It is relatively abundant in meteorites, and some natural enrichment at the earth's surface occurs due to volcanic activity.[3] Distinctive properties include its resistance to chemical attack, excellent high-temperature characteristics, and electrical properties. These are increasingly exploited for industrial applications in the electronic, chemical, and automotive industries in the form of alloys with Pt, Pd, and Rh for automotive catalytic converters, in crucibles, thermocouples, spaceship engines, gas turbines, and spark plugs.[4,5] Its increasing use has also raised the issue of its impact on biogeochemical and environmental cycles[6] as well as human health concerns, driving the demand for analytical methodologies providing baseline data to establish natural levels from which assessment of changes can be reliably made.[5]

Determination of extremely low concentrations of Ir in the environment poses a considerable analytical challenge. Overviews of the main analytical methodologies and sample preparation scenarios, including various preconcentration techniques, to assess such low Ir levels have recently become available.[4,7] Among the variety of techniques, inductively coupled plasma mass spectrometry (ICPMS) has gained a particular popularity due to the speed of analysis and extreme sensitivity of determination of many elements. For some elements, a substantial improvement in detection capability may be provided when coupled to vapor generation (VG) for analyte introduction due to their conversion to a volatile compound (species), separation from the liquid matrix, and efficient gas phase transport to the detector. VG can offer substantially higher analyte introduction efficiency (100% in an ideal case) than is typical for conventional solution pneumatic nebulization (PN, <10%). Other benefits arise due to the removal of the sample matrix in that the analyte is often selectively separated from the liquid phase, eliminating spectral and non-spectral interferences during detection and further contributing to enhanced detection power.

Compared to the mature approach of VG based on chemical reduction of analyte by tetrahydridoborate, with photo-

Received: October 21, 2022
Accepted: January 28, 2023

chemical vapor generation (PVG), volatile analyte species are synthesized during UV irradiation of an aqueous reaction medium typically containing low-molar mass carboxylic acids such as formic and acetic acid.[8,9] The resulting highly reducing radical species ($H^{\bullet}$, $CO_2^{\bullet-}$), and $e_{(aq)}^-$), along with photogenerated $R^{\bullet}$ and CO, subsequently interact with the analyte to form volatile hydrides, carbonyls, or alkylated compounds depending on the analyte and reaction medium used. PVG is still rapidly developing in scope, having added more than 10 new elements in the past 5 years.[10−19] This is also due to the recent introduction of metal sensitizers that significantly increase the PVG efficiency or are even indispensable to initiate PVG of some analytes. Metal sensitizers exhibiting such effects on PVG include: Cd^{2+} ions for As^{3+} and As^{5+},[20] Se^{6+},[21] and W^{6+};[15] Co^{2+} ions for Bi^{3+},[22,23] Cd^{2+},[24] Ge^{4+},[10] Pb^{2+},[25] Sb^{3+},[26] Te^{4+},[27] and Tl^{+};[28] Cu^{2+} ions for Br^-,[29] Cl^-,[19,29] F^-,[14,29] Ir^{3+},[17] and Rh^{3+};[17] Fe^{2+} and/or Fe^{3+} ions for As^{3+},[30] Bi^{3+},[31] Te^{4+},[32] Mo^{6+},[16] Cd^{2+},[33] and Os^{4+};[18] Ni^{2+} ions for Pb^{2+};[25] and V^{4+} and V^{5+} for Te^{4+} and Te^{6+}.[34] A greater effect (additive or synergistic) was reported for several analytes when a combination of two metal sensitizers was employed: namely, Co^{2+} and Cu^{2+} ions for Mo^{6+};[35] Cd^{2+} and Co^{2+} for Os^{4+},[12] Re^{7+},[11] and Ru^{3+};[12,13] and Mn^{2+} and Fe^{2+} ions for Te^{4+}.[36] The mechanism of the action of the metal sensitizers on PVG remains to be fully elucidated, but the latest studies dealing with application of electron paramagnetic resonance spin trapping techniques support the initial thesis[8] that transition metal ions enhance the yield of highly reducing $CO_2^{\bullet-}$ during UV irradiation of HCOOH.[11,27,34,35,37]

The feasibility of PVG of Ir was demonstrated by de Oliveira and Borges[17] within a multi-element study (also devoted to Au, Pd, Pt, and Rh) based on the use of a comparatively inefficient photoreactor (no vacuum UV capability) consisting of two 40 W low-pressure Hg lamps to irradiate a quartz tube through which the sample was passed. With the main focus on seawater analysis, they identified a significant positive effect of Cu^{2+} ions enhancing PVG yield and attained a 20 ng L^{-1} limit of detection (LOD) by coupling PVG sample introduction with ICPMS. In a recent 17-element mechanistic study by Yu et al.,[37] the authors simply adopted the same sample generation medium for PVG of Ir but used an advanced high-efficiency flow-through photoreactor with and without introduction of air segments before and after a zone of liquid sample. The authors estimated the PVG efficiency to be in the range of 60−70% by comparison of the Ir signal intensities with those from the PN-ICPMS of solutions before and after their UV irradiation. No LOD was presented.

The current work was undertaken in an effort to identify PVG conditions that would offer highly efficient and repeatable PVG yields useful for ICPMS detection of Ir and to develop an extremely sensitive analytical methodology for its determination at pg L^{-1} levels (ppq).

EXPERIMENTAL SECTION

Instrumentation. The same PVG system described in our recent study of PVG of Ru,[13] based on a flow injection (FI) mode of operation and coupled to ICPMS, was utilized (see the Supporting Information for a scheme and details on the entire arrangement). Briefly, it consisted of a chemifold fitted with an injection valve (0.5 mL sample loop), a plastic gas−liquid separator (GLS, 15 mL), and a high-efficiency flow-through photoreactor (19 W, Jitian Instruments Co., China). A 200 mL min^{-1} flow of Ar carrier was used to provide the efficient release of volatile Ir species and their transport from the GLS to the ICPMS (see details in Supporting Information).

Detection was achieved using an Agilent 8900 triple-quadrupole ICPMS operating in time-resolved analysis and single-quadrupole modes using either no gas or He gas (4.1 mL min^{-1}) in the reaction/collision cell. Optimal plasma settings for PVG measurements and selected isotopes are summarized in Table S1 of the Supporting Information. If not explicitly stated, all results are based on ^{193}Ir peak area response. Note that no statistically significant difference in optimized parameters, apart from expected sensitivity, was evident when monitoring ^{191}Ir.

Reagents and Materials. Deionized water (DIW, <0.2 μS cm^{-1}, Ultrapur, Watrex) was used for the preparation of all solutions unless otherwise stated. Formic acid (98%, p.a., Lach-Ner, Czech Republic) was used for the formulation of reaction media of various molarities (M, i.e., mol L^{-1}). A commercial stock analytical standard solution of 1024 mg L^{-1} Ir^{3+} (as $IrCl_3$) in 10% (m/v) HCl was obtained from Sigma-Aldrich. Standard solutions containing 870 mg L^{-1} Ir^{3+} and 815 mg L^{-1} Ir^{4+} were prepared by dissolving solid ammonium hexachloroiridate(III) ($(NH_4)_3[IrCl_6]$, Fluka) and ammonium hexachloroiridate(IV) ($(NH_4)_2[IrCl_6]$, Fluka) in 10% (m/v) HCl. The following compounds were used as potential metal sensitizers for PVG: cadmium(II) acetate dihydrate (p.a., Lach-Ner), cobalt(II) acetate tetrahydrate (99.999%, Alfa Aesar), copper(II) acetate monohydrate (Merck), iron(II) acetate (≥99.99%, Sigma-Aldrich), manganese(II) acetate tetrahydrate (p.a., Sigma-Aldrich), and nickel(II) acetate tetrahydrate (p.a., Sigma-Aldrich). Stock solutions of metal sensitizers were prepared by dissolution of these metal acetates in 0.2% (m/v) CH_3COOH and contained 2.5−10 g L^{-1} of individual metals. For interference studies, stock solutions of 1000 mg L^{-1} Au^{3+}, Fe^{3+}, Mn^{2+}, and Pt^{4+} in 1 M HCl and 1000 mg L^{-1} Zn^{2+} in 1 M CH_3COOH were sourced from BDH (UK), 1000 mg L^{-1} Mo^{6+} in 0.5% (m/v) NH_4OH from Absolute Standards, Inc. (USA), 1000 mg L^{-1} Rh^{3+} in 5% (m/v) HCl from Fluka, 1000 mg L^{-1} Pd^{2+} in 5% (m/v) HCl from Sigma-Aldrich, and 1000 mg L^{-1} Cu^{2+} in 2% (m/v) HCl from Analytika (Czech Republic). A 1000 mg L^{-1} solution of As^{3+} in DIW was prepared from arsenic(III)oxide (Lachema, Czech Republic), and 5000 mg L^{-1} Se^{4+} in DIW was prepared from sodium selenite(IV) pentahydrate (Lachema). Other chemicals were sourced as follows: ammonium hydroxide (25%, p.a.), nitric acid (65%, semiconductor grade), and sodium formate from Sigma-Aldrich; acetic acid (99.8%, p.a.), sulfuric acid (96%, chem. pure), and sodium chloride (p.a.) from Lach-Ner; sodium hydroxide (p.a.) from Penta (Czech Republic); hydrochloric acid (35%, Analpure) and ultrapure water (Analpure Ultra) from Analytika; sodium peroxide (≥95%, p.a.) from Carl Roth; and sodium nitrate (Suprapur) from Merck.

Procedure and Conventions. Measurements were conducted in the FI mode using a constant flow of the carrier (reaction) medium propelled by a peristaltic pump. A standard/sample prepared in the reaction medium and spiked with selected sensitizers, if any, was manually injected into the carrier stream at the beginning of a PVG cycle of recording signal intensities. Integration of the signal was stopped after the transient signal returned to the baseline.

Peak area (counts) of the flow injection transients, normalized to the averaged signal from a ^{185}Re internal

https://doi.org/10.1021/acs.analchem.2c04660
Anal. Chem. XXXX, XXX, XXX−XXX

standard (IS) simultaneously admitted by PN over the same measurement time window, was employed as a measure of analyte response. Each result is presented as the average of at least three peak area replicates with an uncertainty given as ± 1 standard deviation (SD) or combined uncertainty where results are relative. Overall PVG efficiency is defined as the fraction of the analyte that is converted to volatile species, released to the gas phase, and transported to the plasma. Nebulization efficiency represents the fraction of the analyte introduced into the spray chamber and transported to the plasma. Overall PVG efficiency was determined according to our previously published procedure[13,15,22,33] and is the product of a sensitivity enhancement factor and absolute nebulization efficiency. The enhancement factor is defined as the ratio of the peak area sensitivity obtained with FI-PVG sample introduction to that arising from FI-PN during their concurrent operation, i.e., both measured under exactly the same plasma conditions. The nebulization efficiency was determined under optimal settings of the ICPMS (Table S1) using a modified waste collection method (sometimes called a dynamic mass flow approach).[38] To provide an immediate indication of a state of optimization of PVG of Ir (or other elements), the overall PVG efficiency was estimated for each measurement by comparison of peak area sensitivity obtained with FI-PVG and FI-PN. These values are given in the text without a corresponding uncertainty.

For comparison, overall PVG efficiency was also quantified using an indirect approach based on determination of the amount of Ir in the waste solution after PVG using conventional PN-ICPMS (details on this procedure are available in ref 39).

Sample Preparation. Five natural water samples comprising various matrices were analyzed. A spring water sample was collected at a chapel of the Bohosudov Church (Krupka u Teplic, Czech Republic); a river water sample was collected from the Vltava River in Prague, and lake water was sampled from the Lipno Reservoir, the largest water feature in the Czech Republic. Additionally, two seawater samples (I and II) were collected at two locations on the Istrian Peninsula in Croatia (Camping Mon Perin and Sveta Marina). Samples were filtered through a 0.45 μm PTFE filter and prepared for parallel analysis by FI-PVG-ICPMS (prepared in 4 M HCOOH containing 10 mg L^{-1} Co^{2+} and 25 mg L^{-1} Cd^{2+}) and by conventional PN-ICPMS/MS (prepared in 2% (m/v) HNO_3).

A pulverized NIST Standard Reference Material 2556 – Used Auto Catalyst (Pellets) was decomposed by means of sodium peroxide fusion. Approximately 0.4 g of SRM 2556 was mixed with 2 g of Na_2O_2 in a sintered alumina crucible (27 mL). The heating program was as follows: 15 min at 220 °C followed by 30 min at 620 °C. After cooling, the vitreous sample mass was carefully dissolved in 20 mL of 5 M HCl and 30 mL of water by alternately adding water and 5 M HCl in 5 mL increments. This digest was further diluted and prepared for parallel analysis by FI-PVG-ICPMS (in 4 M HCOOH containing sensitizers) and by conventional PN-ICPMS/MS (in 2% (m/v) HNO_3).

■ RESULTS AND DISCUSSION

PVG without Additives. The PVG reaction was first examined using only an HCOOH medium in the absence of metal ion sensitizers or other additives in order to establish a "baseline" performance. The most important parameters influencing PVG were investigated, including HCOOH concentration and sample irradiation time (IT), which is inversely proportional to the flow rate of the sample through the photoreactor. Using a flow rate of 1.5 mL min^{-1} through the photoreactor (IT = 29 s), the effect of HCOOH concentration was examined in the range of 2–20 M HCOOH. Sensitivity gradually increased with higher HCOOH concentrations and reached a maximum at 18 M HCOOH (see Figure S2 in the Supporting Information). These signals were confirmed to arise from PVG processes because absolutely no signals were detected at 4, 10, and 18 M HCOOH when the UV lamp was not powered. From a comparison of peak area response using a 1 μg L^{-1} solution Ir^{3+} in 2% (m/v) HNO_3 introduced via the same 500 μL sample loop and FI-PN mode, overall PVG efficiency at 18 M HCOOH was estimated to be ≈9%. The effect of IT was subsequently investigated at three concentrations of HCOOH (10, 14, and 18 M HCOOH) by altering the sample flow rate in the range of 0.5–2.5 mL min^{-1} (Figure 1).

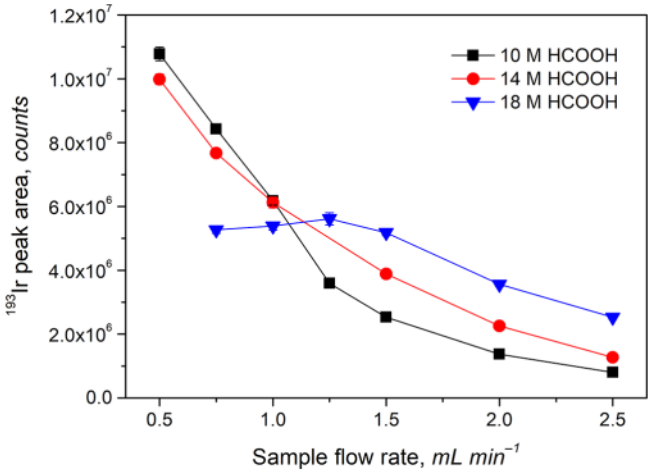

Figure 1. Effect of sample flow rate at various concentrations of HCOOH in the reaction medium on peak area response from 200 ng L^{-1} Ir^{3+}. Uncertainties expressed as SD ($n \geq 3$) are sufficiently small that they cannot be discerned from the data points in some cases.

It is evident that for 10 and 14 M HCOOH the sensitivity gradually increases down to a flow rate of 0.5 mL min^{-1} (IT = 87 s) but no maxima are identified in the tested range. The decline at higher flow rates was proven to be due to insufficient irradiation of the sample and not to a lower efficiency of the gas–liquid separation process in the GLS (see experimental results confirming this conclusion in the Supporting Information). The overall PVG efficiency for 10 M HCOOH at 0.5 mL min^{-1}, representing the conditions with the highest sensitivity noted in Figure 1, was estimated to be ≈18%. In contrast to 10 and 14 M HCOOH media, the dependence for 18 M HCOOH is different, reaching a maximum at 1.25 mL min^{-1}, wherein a slight decline of sensitivities follows at both lower and higher sample flow rates. This can be explained by an increased production of bubbles (comprising CO, CO_2, and H_2) from UV homolysis of HCOOH in the photoreactor, clearly observed at flow rates ≤1.25 mL min^{-1}. Bubble expansion tends to expel the reaction medium from the photoreactor, and IT likely effectively remains the same in the 0.75–1.25 mL min^{-1} range. No significant bubble formation is observed at any sample flow rate using 10 M HCOOH while

https://doi.org/10.1021/acs.analchem.2c04660
Anal. Chem. XXXX, XXX, XXX–XXX

their formation was initiated at ≤0.75 mL min^{-1} using 14 M HCOOH. Signals generated from 6, 10, and 14 M CH_3COOH media at 1.5 mL min^{-1} were 200−250-fold lower than those obtained with 6, 10, and 14 M HCOOH. The addition of 1 or 2 M CH_3COOH to 9 and 8 M HCOOH also did not provide any enhancement effect on PVG of Ir in comparison to 10 M HCOOH alone. Hence, CH_3COOH is not a suitable medium for PVG of Ir, consistent with observations on PVG of other transition metals with the exception of Os[18] and Re.[11] For the latter, CH_3COOH was fruitful only when used in combination with HCOOH.

These pilot experiments demonstrated that PVG of Ir necessitates rather high concentrations of HCOOH and long ITs when conducted without additives. Generally, high concentrations of HCOOH are not suitable due to the accompanying dilution of real samples by added HCOOH prior to analysis.[39] Potential improvement in overall PVG efficiency could possibly be realized at 10 and 14 M HCOOH by further increase in the IT. This, however, is not well tolerated in this flow system because the flow injection peaks become too broad even at flow rates of ≤1 mL min^{-1}, requiring long integration times and limitations on sample throughput. In order to substantially enhance the overall PVG efficiency while keeping rather short IT and relatively low HCOOH concentration in the reaction medium, the effect of metal sensitizers or other additives influencing pH was investigated.

Effect of pH. Similar to PVG of Fe, Co, and Ni,[39−44] an increase in pH of the reaction medium exerted a significant effect on the PVG efficiency (Figure S3). The effect of pH was examined by varying the volume of added liquid ammonia ($NH_3·H_2O$) to partially neutralize solutions of 10 M HCOOH. The resulting reaction media containing 0−5 M of formed $HCOONH_4$ in 5−10 M of "unreacted" HCOOH were used as the carrier and for preparation of the Ir^{3+} standard that was injected into a continuous stream of this carrier medium. A maximum of peak area was reached at pH = 3.4 and 3.7, corresponding to media containing 4 M $HCOONH_4$ in 6 M HCOOH and 5 M $HCOONH_4$ in 5 M HCOOH, respectively. This provided an approximately 4.5-fold signal increase relative to only 10 M HCOOH (pH = 1.38), corresponding to an overall PVG efficiency of ≈19%. The effect of IT was then examined at pH = 3.4, i.e., using a mixture of 4 M $HCOONH_4$ and 6 M HCOOH (Figure S4). Analogous to the reaction media containing only 10 M or 14 M HCOOH (cf. Figure 1), no maximum sensitivity was reached in the range of 0.5−2.5 mL min^{-1} and the sensitivity exponentially increased with lower flow rates and corresponding longer ITs. Nevertheless, the estimated overall efficiency of ≈71% at 0.5 mL min^{-1} suggests the potential for PVG becoming highly efficient.

The same enhancement effect on peak area sensitivity was observed when liquid $NH_3·H_2O$ was replaced with solid NaOH to partially neutralize 10 M HCOOH. Interestingly, an overall PVG efficiency of ≈8% can be reached when PVG is conducted from 10 M HCOONa (pH = 9.4) prepared by dissolution of solid HCOONa in DIW, which represents around 2-fold increase in comparison to PVG from 10 M HCOOH (pH = 1.38). It should be noted, however, that the preparation of such reaction media from highly concentrated HCOOH and high volumes of ammonia or large masses of NaOH is laborious as the solutions need to be cooled during preparation, and it also introduces a high risk of contamination. Due to such limitations, pH adjustment of the reaction medium was not undertaken with any subsequent experiments.

PVG in the Presence of Metal Ion Sensitizers. The possibility of substantial enhancement yet available in overall PVG efficiency was examined by the addition of various metal ion sensitizers. The metals were added only to the Ir^{3+} standard in 10 M HCOOH and not to the carrier (10 M HCOOH) into which the standard was injected. Metal ions (Cd^{2+}, Co^{2+}, Cu^{2+}, Fe^{2+}, and Ni^{2+}) were chosen on the basis of their previously reported efficacy on PVG of various analytes.[11,17] In addition, Mn^{2+}, recently reported effective for PVG of Te^{4+}, was tested.[36] The effects of various concentrations of individual metal ions on PVG of Ir at a sample flow rate of 1.5 mL min^{-1} are shown in Figure 2.

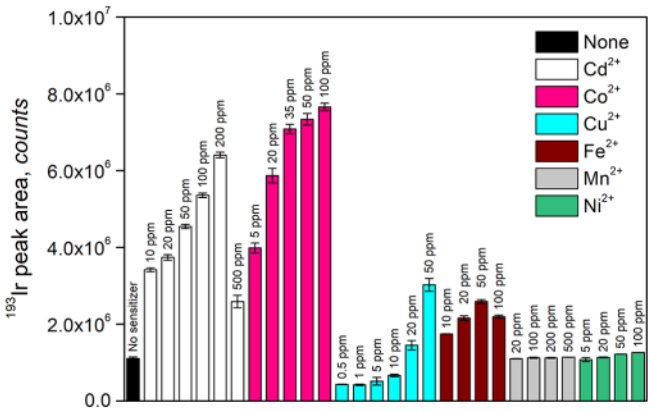

Figure 2. Influence of various metal ion concentrations on PVG response from 100 ng L^{-1} Ir^{3+} in 10 M HCOOH at a sample flow rate of 1.5 mL min^{-1}. Uncertainties are expressed as SD ($n \geq 3$).

The most notable effects were exhibited by Co^{2+} and Cd^{2+} ions, while other ions had significantly less impact. The estimated overall PVG efficiency of ≈30% was achieved using 100 mg L^{-1} Co^{2+}, whereas ≈25% was reached using 200 mg L^{-1} Cd^{2+}. These respectively constituted approximately 6.9- and 5.8-fold enhancements in comparison to the conditions without sensitizer using only 10 M HCOOH (efficiency typically 4−5%). Higher concentrations of Co^{2+} were not tested so as not to overload the plasma/interface with volatile Co species (see below) and because a plateauing effect seemed to be achieved at concentrations of ≥100 mg L^{-1} Co^{2+}.

A quite unique effect was evident for Cu^{2+} in that lower concentrations (0.5−5 mg L^{-1}) interfered with PVG of Ir, decreasing the sensitivity by about 2-fold, but at higher concentrations, it curiously enhanced the PVG efficiency. Furthermore, as opposed to other metal ion sensitizers, enhanced production of bubbles was observed when samples containing 20 and 50 mg L^{-1} Cu^{2+} were irradiated. Nevertheless, higher concentrations of added Cu^{2+} were responsible for increased blanks and also memory effects. Copper can be deposited on the conduits of the photoreactor during irradiation[45] and change irradiation characteristics over time. Note that the impact of added Cu^{2+} observed here is different from that reported by de Oliveira and Borges,[17] likely because of the significantly different conditions of sample irradiation available with their photoreactor. As for added Fe^{2+}, this sensitizer was not particularly effective and maximum overall PVG efficiency of ≈10% was attained at 50 mg L^{-1}.

https://doi.org/10.1021/acs.analchem.2c04660
Anal. Chem. XXXX, XXX, XXX−XXX

Absolutely no or only slight enhancement was observed at 20−500 mg L^{-1} Mn^{2+} and 5−100 mg L^{-1} Ni^{2+}.

Only Co^{2+} and Cd^{2+} ions appear to be attractive sensitizers for PVG of Ir. Following the recent study of PVG of Ru^{3+},[13] wherein a strong synergistic effect of both ions was identified, the impact of various combinations of added Co^{2+} and Cd^{2+} sensitizers was further examined, as illustrated in Figure 3.

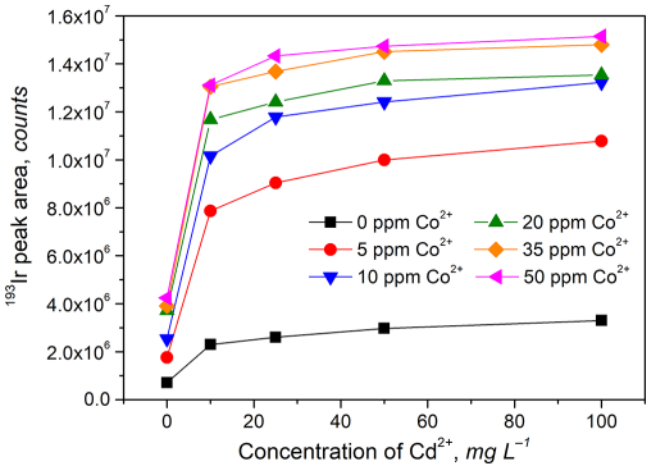

Figure 3. Effect of various combinations of Co^{2+} and Cd^{2+} ions present in 10 M HCOOH on PVG from 50 ng L^{-1} Ir^{3+} at a sample flow rate of 1.5 mL min^{-1}. Uncertainties expressed as SD ($n \geq 3$) are sufficiently small that they cannot be discerned from the data points.

It is evident that the overall PVG efficiency increases with both Co^{2+} and Cd^{2+} concentrations and when used in combination reach plateaus at 35−50 mg L^{-1} Co^{2+} and 50−100 mg L^{-1} Cd^{2+}. The estimate of overall efficiency suggests almost quantitative yield (≥90%) under these PVG conditions. Further experiments also revealed a similar synergistic effect from the co-presence of Fe^{2+} and Cd^{2+} ions wherein a combination of 50 mg L^{-1} Fe^{2+} and 200 mg L^{-1} Cd^{2+} led to an overall PVG efficiency of ≈82%. This combination was not pursued further as the required concentration of Fe^{2+} was too high (see below). Conversely, addition of 50 mg L^{-1} Fe^{2+} to 35 mg L^{-1} Co^{2+} had absolutely no positive influence relative to that from only 35 mg L^{-1} Co^{2+}.

A significant concern arises with use of metal sensitizers for PVG in that their volatile species may be co-generated concurrently with the analyte, resulting in high loading of the ICP due to their typically mg L^{-1} concentrations, which is unfavorable for long-term use. With respect to those sensitizers having a significant positive effect, both Co^{2+} and Fe^{2+} result in co-generation of volatile $Co(CO)_4H$ and $Fe(CO)_5$ species, respectively.[46,47] Negligible and irregular response during PVG was observed for Cd (m/z 111) if used as the lone sensitizer. The same result was earlier reported for PVG of W sensitized by addition of 500 mg L^{-1} Cd^{2+},[15] although some contribution from direct PVG action can be expected.[24,33] The situation slightly improved when Cd^{2+} was used in combination with Co^{2+}, but its estimated overall PVG efficiency remained never higher than 0.01%, even when a sample flow rate of 0.75 mL min^{-1} (IT = 58 s) was employed.

Re-Optimization of the PVG System. A compromise combination of 10 mg L^{-1} Co^{2+} and 25 mg L^{-1} Cd^{2+} was chosen for further experiments to maintain the transfer of Co to the ICP as low as possible. The main PVG conditions, such as HCOOH concentration and IT, were thus re-optimized. The HCOOH concentration was varied in the range of 0.005−16 M HCOOH, revealing a remarkable impact on peak area sensitivity (Figure S5). No dramatic changes in sensitivity were evident over the broad range of 0.1−8 M HCOOH, and only a slight increase toward the maximum at 1 M HCOOH was observed. This dependence is completely different from that shown in Figure S2, wherein a gradual increase in sensitivity occurred with increase in HCOOH concentration up to 18 M for PVG in the absence of sensitizers. Surprisingly, PVG of Ir now remains highly efficient even at very low HCOOH concentrations, wherein the overall efficiency ranges 57−88% for 0.005−0.1 M HCOOH. The Co^{2+} and Cd^{2+} sensitizers are thus extremely beneficial, and their presence significantly alters the course of PVG possibly via an enhancement the yield of highly reducing $CO_2^{\bullet-}$ during UV irradiation of HCOOH,[11,27,34,35,37] which likely leads to more efficient reduction of Ir^{3+} to Ir^0 and subsequent capture of co-generated CO molecules delivered from photolytic homolysis of HCOOH. However, the irritating question arises as to why so little acid remains sufficient to promote such efficient PVG of Ir. A more definitive explanation is not available at this time as the phenomenon requires significantly further investigation.

With respect to such a broad range of suitable HCOOH concentrations for efficient PVG in the presence of sensitizers, the selection of the optimal concentration for routine use and analytical applications presents some complications. Lower concentrations of HCOOH definitely offer some advantages, including lower risk of contamination and less dilution of real water samples with concentrated HCOOH.[39] Conversely, tolerance toward interferences may be compromised due to a lower concentration of generated $CO_2^{\bullet-}$ and $e_{(aq)}^-$ as well as less CO for synthesis of Ir carbonyl. Selection of the optimal HCOOH concentration was thus finally based on the tolerance of the system toward the presence of HNO_3 as it represents the most powerful scavenger of free radicals during PVG of many analytes.[48] The impact of 0.1−10 mM HNO_3 at 0.1, 1, 4, and 10 M HCOOH on PVG of Ir is demonstrated in Figure S6. Without doubt, higher tolerance toward HNO_3 is obtained at higher concentrations of HCOOH. A 4 M HCOOH medium was chosen as a compromise for further experiments, offering reasonable tolerance toward interferences and low sample dilution inevitably accompanying preparation of real samples in HCOOH while also giving rise to a further 7% enhancement in sensitivity over that realized for 10 M HCOOH (cf. Figure 3 and Figure S5).

The dependence of peak area sensitivity on sample flow rate in 4 M HCOOH (Figure S7) became rather featureless, with a plateau in the range of 0.75−1.5 mL min^{-1} (cf. Figure 1 and Figure S4). This indicates that the overall PVG efficiency must be close to 100% (see below) because there is no possibility for further significant improvement using higher ITs.

Figures of Merit. The following PVG conditions were selected for routine use: 4 M HCOOH as the reaction medium delivered at 1.5 mL min^{-1} flow rate (IT = 29 s) and the further addition of 10 mg L^{-1} Co^{2+} and 25 mg L^{-1} Cd^{2+} to the standard/sample. A typical FI signal from 50 ng L^{-1} Ir^{3+} is displayed in Figure 4. It is evident from the transients that the FI signals do not suffer from serious tailing, which allows for a satisfactory sampling frequency of 15 samples h^{-1} at concentration levels ≤50 ng L^{-1}.

Although the PVG efficiency was estimated daily by comparison of the replicate peak areas measurements of one

https://doi.org/10.1021/acs.analchem.2c04660
Anal. Chem. XXXX, XXX, XXX−XXX

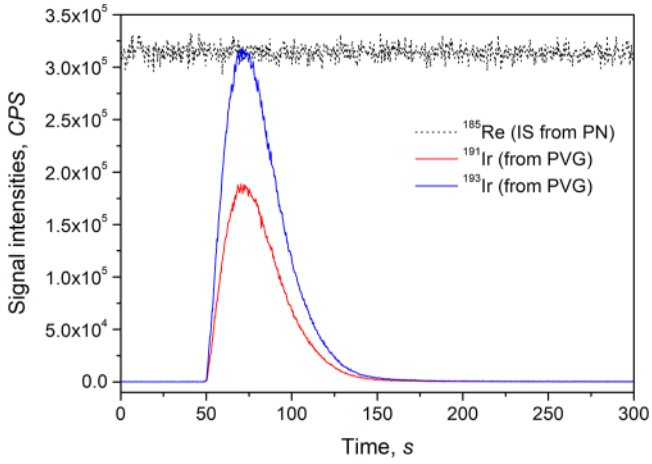

Figure 4. Typical PVG transient signals from 50 ng L^{-1} Ir^{3+} generated from 4 M HCOOH after the addition of 10 mg L^{-1} Co^{2+} and 25 mg L^{-1} Cd^{2+} as sensitizers. Continuous signal of ^{185}Re (dotted line) from concurrent nebulization of a solution of 10 μg L^{-1} Re is included for comparison.

standard concentration obtained with both FI-PVG and FI-PN processing under the same plasma conditions, the precise value of overall PVG efficiency under the chosen optimal PVG conditions was determined from a comparison of the slopes of calibration functions for FI-PVG (0, 10, 25, and 50 ng L^{-1} Ir^{3+}) and FI-PN (0, 50, 250, and 1000 ng L^{-1} Ir^{3+}). The sensitivity enhancement factor reached 10.50 ± 0.06, while the nebulization efficiency determined by the dynamic mass flow approach was 8.44 ± 0.04%. These values result in an overall calculated PVG efficiency of 88.6 ± 0.6%. A very similar value of 88.0 ± 2.2% was determined by an indirect approach following an assessment of the Ir remaining in the waste after FI-PVG of a 10 μg L^{-1} solution of Ir^{3+} containing added sensitizers. Although this determination had to be carried out at ≥200-fold higher concentration, it provided supporting evidence that the remaining fraction (11−12%) of Ir is not firmly deposited in the conduits of the generator.

An increase to 91−95% can be easily obtained at lower HCOOH concentrations (1−2 M; Figure S5) or with the use of higher concentrations of metal sensitizers, especially Co^{2+} (Figure 3). An overall PVG efficiency of 97.5 ± 0.7% can also be achieved if the sensitizers (10 mg L^{-1} Co^{2+} and 25 mg L^{-1} Cd^{2+}) are added not only to the Ir^{3+} standard in 4 M HCOOH but also to the reaction medium serving as the carrier. In the case when an Ir^{3+} standard containing sensitizers is injected into a carrier stream comprising only 4 M HCOOH, dispersion of the analyte as well as metal sensitizers in the photoreactor conduit cannot be avoided and the concentrations of metal sensitizers at the leading and falling edges of the analyte zone become lower during their transport through the photoreactor. Nevertheless, the potential slight increase in overall PVG efficiency is not worth incurring problems associated with overloading the plasma with high metal concentrations of continuously co-generated Co.

The PVG methodology is characterized by excellent precision (RSD); a repeatability of 1.0% (n = 15) in the peak area was obtained for a quality control check standard of 50 ng L^{-1} Ir^{3+} used throughout the course of one measurement day. All calibration functions for both ^{191}Ir and ^{193}Ir isotopes using 0, 1, 2, 4, 10, 25, and 50 ng L^{-1} Ir^{3+} standards measured using either a no gas mode or He mode in the reaction/collision cell were linear (R^2 > 0.9999). Sensitivities in He mode were approximately 35% lower than those in the no gas mode due to ion scattering. Using no gas mode, outstanding LODs (3σ, n = 11) of 3 pg L^{-1} (1.5 fg absolute) were reached for both ^{191}Ir and ^{193}Ir, whereas using He mode provided LODs (n = 11) of 6 pg L^{-1} (3 fg absolute). A typical small but persistent peak-shaped signal comprising single to a few tens of counts for 0.1 s dwell time characterized blank measurements. The LODs are thus driven by the variance of the peak area of this blank signal, the concentration of which corresponded to 0.015−0.03 ng L^{-1} provided that the PVG system was clean and not contaminated by prior measurement of a sample containing >10 ng L^{-1} Ir. The source of this blank was, in part, derived from the added Co^{2+} sensitizer solution. Sub-boiling distillation of HCOOH or use of ultrapure water from a commercial supplier provided no improvement in blank values.

The influence of the oxidation state of Ir (Ir^{3+} vs Ir^{4+}) on PVG efficiency was also examined using standards prepared from solid $(NH_4)_2[IrCl_6]$, i.e., Ir^{4+}, and $(NH_4)_3[IrCl_6]$, i.e., Ir^{3+}. Compared to the sensitivity obtained using a commercial analytical standard (as $IrCl_3$), an identical response (100 ± 2%) was verified with Ir solutions prepared using both solid salts. The redox stability of these Ir species in prepared reaction media (4 M HCOOH with or without sensitizers) was examined by UV−vis spectrometry based on use of 5 mg L^{-1} Ir solutions. No decline in intensity of the absorption maxima at 305, 418, 435, and 488 nm, indicating the presence of $[IrCl_6]^{2-}$,[49] was identified over the course of 1 week and vice versa, and no appearance of such bands was found for aging a similar Ir^{3+} standard. Hence, the redox stability of the Ir species in the prepared reaction media containing sensitizers seems not to be an issue and the sequential reduction of Ir^{4+} to Ir^{3+} to Ir^0 can be confirmed as due to the action of PVG.

For comparison, LODs (n = 13) for conventional PN-ICP-MS/MS employing an autosampler and continuous flow steady-state measurements were evaluated for ^{191}Ir and ^{193}Ir. Using standard no gas mode, 0.07 and 0.06 ng L^{-1}, respectively, were obtained, whereas in He mode, these values were 0.09 and 0.06 ng L^{-1}, respectively. It is evident that FI-PVG-ICPMS surpasses conventional PN-ICPMS/MS in terms of LODs by more than one order of magnitude, which arises as a result of the more than 10-fold increase in the efficiency of analyte introduction into the plasma.

The substantial performance benefits arising from PVG of Ir are a direct consequence of its introduction as a gas phase species.[50] It is assumed that the volatile species synthesized herein may be $Ir(CO)_4H$, $Ir_2(CO)_8$ or $Ir_4(CO)_{12}$ based on the use of HCOOH giving rise to only hydrided/carbonylated adducts. In relatively older studies, formation of $Ir(CO)_4H$ was reported when water containing $IrCl_3$ was used for the preparation of other iridium carbonyls and detected as a very volatile compound,[51] including the direct evidence by Whyman,[52] who used IR spectroscopy to investigate reactions of $Ir_4(CO)_{12}$ under various pressures of CO and H_2 and found no evidence for formation of $Ir_2(CO)_8$.[53] To the best of our knowledge, successful GC−MS detection of any iridium carbonyl has not yet been achieved (including our most recent attempts),[54] and there is also no MS spectrum available in the NIST database.[55] Hence, identification of the product of PVG may be challenging despite its relatively good stability based on experience generated in this study.

Interferences. Interference effects from HNO_3, HCl, and H_2SO_4 arising under compromised optimal PVG conditions

https://doi.org/10.1021/acs.analchem.2c04660
Anal. Chem. XXXX, XXX, XXX−XXX

were examined. Consideration of their possible application with the proposed methodology arises from their use during digestion and/or stabilization of samples. Figure 5 shows that a

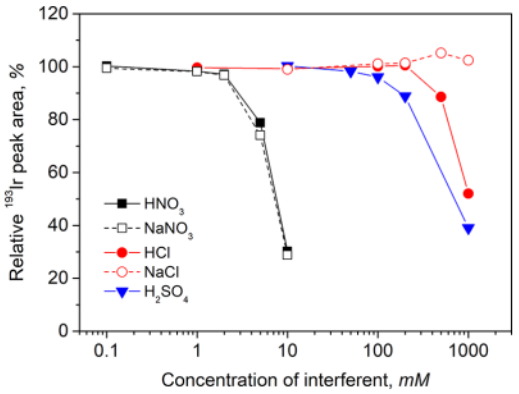

Figure 5. Relative effects of added inorganic acids and salts on PVG from 50 ng L^{-1} Ir^{3+} prepared in 4 M HCOOH containing 10 mg L^{-1} Co^{2+} and 25 mg L^{-1} Cd^{2+} as sensitizers. Combined uncertainty associated with individual data points is lower than 2% in all cases.

serious suppressive effect occurs for HNO_3, wherein concentrations of 5 and 10 mM cause 26 and 71% decreases in sensitivity, respectively. (Note: The same dependence is actually presented in Figure S6, where tolerance toward HNO_3 was compared for various concentrations of HCOOH). This interference seems to be driven by the NO_3^- anion because the impact of added $NaNO_3$ salt was completely identical. The PVG system was, by almost two orders of magnitude, more tolerant to the presence of H_2SO_4 in that a significant decrease in sensitivity (by 11%) occurred at 200 mM. Tolerance toward Cl^- anion was excellent, which can be demonstrated by a significant decrease (>10%) in response only at concentrations higher than 500 mM (for HCl) and by absolutely no negative interference from NaCl up to 1 M. The lower tolerance toward HCl compared to NaCl is likely caused by a concurrent change in sample pH. To the best of our knowledge, such excellent tolerance toward HCl and NaCl has not been reported for PVG of any other transition metal and encourages a direct determination of dissolved Ir in complex matrices such as seawater (≈0.54 M Cl^-) without any required dilution.

In addition to inorganic acids, the effect of potential co-existing transition metals that can be present in typical prepared samples of interest containing Ir (i.e., Mn^{2+}, Fe^{3+}, Cu^{2+}, Zn^{2+}, Mo^{6+}, Rh^{3+}, Pd^{2+}, Pt^{4+}, and Au^{3+}) and metalloids (As^{3+} and Se^{4+}) was examined in the range of 0.01−10 mg L^{-1} (see Table S3 in the Supporting Information). No negative interference was found for Mn^{2+}, Fe^{3+}, Zn^{2+}, and Mo^{2+} present in prepared samples at levels up to 10 mg L^{-1}. With the exception of Pd^{2+} inducing a 13% suppression in response at only 0.1 mg L^{-1}, a significant decrease in sensitivity (>10%) was identified for other elements at 1 mg L^{-1} levels, namely, by 20% for Cu^{2+}, 70% for As^{3+}, 31% for Se^{4+}, 36% for Pt^{4+}, and 42% for Au^{3+}. It was remarkable that the negative interference from Cu^{2+} ions (around 50%) observed at 0.5−5 mg L^{-1} during the assessment of potential sensitizers (Figure 2) was alleviated under conditions arising with the recommended sensitizers; recovery in the presence of 10 mg L^{-1} Cu^{2+} actually increased to 91%. This behavior is in line with the already described effect of higher concentrations of Cu^{2+} on PVG without added Co^{2+} and Cd^{2+} as sensitizers.

Application to Real Samples. Verification of the accuracy of the developed methodology was challenging due to an absolute lack of certified reference materials with specified Ir content, likely because Ir concentrations in common environmental samples are below detection capabilities of the majority of analytical methods. It is possible that Ir may have become a new component of auto catalytic converters, such as iridium-containing units for direct injection engines manufactured by Mitsubishi of Japan.[4] NIST SRM 2556 (Used Auto Catalyst) was thus chosen to validate the accuracy of the developed methodology. SRM 2556 is certified only for Pb and other PGEs, i.e., Pt (697.4 mg kg^{-1}), Pd (326 mg kg^{-1}), and Rh (51.2 mg kg^{-1}), but Vobecký et al.[56] earlier reported an estimate of 19 μg kg^{-1} Ir by instrumental activation analysis when utilizing a coincidence spectrometer. As Ir may be present in SRM 2556 as a metallic impurity that is resistant to attack by all acids, including aqua regia, sample preparation excludes the use of conventional wet acid digestion techniques for solubilization.[57] Peroxide fusion at 620 °C was thus applied for sample preparation. Fused Na_2O_2 oxidizes Ir to IrO_2 that is subsequently dissolved in dilute HCl and converted to $[IrCl_6]^{4-}$, resulting in an overall 125-fold dilution of the sample (see the Experimental Section). As discussed earlier, the presence of Ir^{4+} species is irrelevant for PVG, and Ir^{3+} standards can be confidently employed for calibration and determination of total Ir by FI-PVG-ICPMS. An aliquot of the digest was diluted a further 100-fold with 4 M HCOOH containing 10 mg L^{-1} Co^{2+} and 25 mg L^{-1} Cd^{2+} as sensitizers and subjected to FI-PVG-ICPMS using He mode detection. The Ir content was quantified by external calibration and corrected for total digestion blank yielding 20.1 ± 0.1 μg kg^{-1}, whereas 20.9 ± 0.2 μg kg^{-1} was obtained by use of the standard additions technique (comprising 1 and 2 ng L^{-1} spiked concentrations), confirming good recovery of 96 ± 1%. It is noteworthy that direct analysis of the digested diluted matrix presented by SRM 2556 can be undertaken using calibration against external standards because the concentrations of all potential interfering ions are at levels at which they exert no significant impact (Table S3). (Note: Final concentrations of 56 μg L^{-1} for Pt, 26 μg L^{-1} for Pd, and 4 μg L^{-1} for Rh can be expected taking into account a total dilution factor of 12,500).

For comparison, a second aliquot of the sample digest was diluted 20-fold with 2% (m/v) HNO_3, yielding a solution containing ≈0.3% dissolved NaCl, which was subjected to determination by conventional PN-ICP-MS/MS using both no gas and He modes of the reaction/collision cell and matrix matched calibration. Values of 21.4 ± 1.0 μg kg^{-1} and 21.4 ± 1.2 μg kg^{-1} were obtained using ^{191}Ir for evaluation in no gas and He mode, respectively, whereas significantly higher values of 29.2 ± 0.8 and 26.9 ± 2.0 μg kg^{-1} resulted when using ^{193}Ir for evaluation. The reason for this discrepancy is likely due to relatively high Pt content in SRM 2556 causing tailing (abundance sensitivity) interferences from adjacent ^{194}Pt (natural abundance 32.97%) and ^{192}Pt (0.782%), especially affecting the ^{193}Ir isotope despite the "high" resolution setting of ICPMS/MS used (see Table S2). It should be noted that this type of spectral interference does not occur with FI-PVG because the PVG efficiency for Pt at 1 μg L^{-1} under conditions optimal for Ir was found to be negligible (≈0.23%). Interestingly, the PVG efficiencies of the other two PGEs present at high concentrations and certified in SRM 2556 were also tested and found to be very low, reaching ≈0.07% for Pd

https://doi.org/10.1021/acs.analchem.2c04660
Anal. Chem. XXXX, XXX, XXX−XXX

and ≈0.16% for Rh. With the exception of the result obtained with conventional PN-ICP-MS/MS using ^{193}Ir for evaluation, the results for Ir content in SRM 2556 agree very well with the earlier value reported by Vobecký et al.[56]

The practical feasibility of determination of dissolved Ir (as Ir^{3+} and Ir^{4+}) at extremely low concentrations was also examined by a direct analysis of five water samples of different matrix complexity. No dilution of the water samples was required except for the addition of concentrated HCOOH and solutions of sensitizers (final dilution factor of only 1.19). The water samples were analyzed by FI-PVG-ICPMS in He mode. Recoveries were calculated from the ratio of slopes of the standard additions (0, 1 and 2 ng L^{-1} Ir spikes added) versus external calibration functions (0, 1 and 2 ng L^{-1} standards). Excellent recovery in the range of 99−102% was achieved for all five samples (Table 1), including a seawater that contains

Table 1. FI-PVG-ICPMS Determination of Dissolved Ir in Water Samples

samples	found (ng L^{-1})	recovery[a]
spring water	<0.007[b]	99 ± 2
river water	<0.007[b]	100 ± 1
lake water	<0.007[b]	99 ± 1
seawater I	0.007[b] < x < 0.024[c]	102 ± 1
seawater II	0.007[b] < x < 0.024[c]	99 ± 2

[a]Spike recovery = slope of standard additions (no addition, 1 and 2 ng L^{-1} spiked to a sample prepared in the reaction medium containing sensitizers)/slope of external calibration (0, 1, and 2 ng L^{-1}) × 100 (%). [b]LOD = 0.007 ng L^{-1} (0.006 ng L^{-1} corrected for dilution factor of 1.19 introduced by preparation of water sample in the reaction medium). [c]LOQ = 0.024 ng L^{-1} (0.020 ng L^{-1} corrected for dilution factor of 1.19 introduced by preparation of water sample in the reaction medium).

≈0.54 M Cl^-. This is in line with the data presented in Figure 5, wherein a tolerance to NaCl is demonstrated even up to 1 M. In parallel, the determination of Ir was attempted by conventional PN sample introduction ICPMS/MS. Results confirmed undetectable levels of dissolved Ir in spring, river, and lake water (below LODs). Seawater samples could not be examined via PN introduction due to the necessity of additional dilution, resulting in further degradation of LODs.

CONCLUSIONS

High PVG efficiency of Ir was achieved under various conditions. If conducted in the absence of metal ion sensitizers, excessive IT appears necessary, which is not feasible using a flow setup; a "stop-flow" mode of operation could be more suitable for this purpose. A substantial enhancement in PVG can be obtained by increasing pH of the reaction medium, although this still requires a lengthy IT or by addition of Co^{2+} and Cd^{2+} ions as sensitizers which synergistically enhance the process. The latter approach was found more practical for analytical applications and also led to an overall PVG efficiency close to 100%.

Excellent repeatability and LODs in the range of 3−6 pg L^{-1} were achieved. These LODs are without doubt the best reported for any element using any VG technique without resorting to prior preconcentration. In addition, excellent tolerance toward chloride anion predestines this method for direct analyses of matrices that would otherwise require significant dilution preceding determination by conventional PN-ICPMS or that of samples following peroxide fusion necessitated for dissolution of metallic Ir.

The variety of real samples selected for analysis in this study was limited in scope due to the non-availability of matrix reference materials certified for Ir content. Consequently, corresponding interference studies have likewise been constrained to reflect the composition of only the real samples examined. Appropriately, it is incumbent on the users of this PVG methodology to first verify the recovery of spikes so as to determine the severity of potential interference encountered with uncharacterized matrices before resorting to use of external calibration for quantitation. Both the method of additions as well as isotope dilution approaches may be confidently used as spectral interferences should be absent.

ASSOCIATED CONTENT

Supporting Information

The Supporting Information is available free of charge at https://pubs.acs.org/doi/10.1021/acs.analchem.2c04660.

Details on instrumentation; scheme of PVG arrangement coupled to ICPMS; ICPMS parameters for FI-PVG and for conventional PN used for real sample analysis; experiments dealing with release and transport of volatile species; effect of HCOOH concentration without additives; effect of pH and sample flow at pH = 3.4 of the reaction medium; influence of HCOOH concentration and sample flow rate using Co^{2+} and Cd^{2+} as sensitizers; relative effects of added HNO_3 in various HCOOH media containing Co^{2+} and Cd^{2+} as sensitizers; influence of various co-existing ions (PDF)

AUTHOR INFORMATION

Corresponding Author

Stanislav Musil − *Institute of Analytical Chemistry of the Czech Academy of Sciences, 602 00 Brno, Czech Republic;* orcid.org/0000-0001-8003-0370; Email: stanomusil@biomed.cas.cz

Authors

Eva Jeníková − *Institute of Analytical Chemistry of the Czech Academy of Sciences, 602 00 Brno, Czech Republic; Faculty of Science, Department of Analytical Chemistry, Charles University, 128 43 Prague, Czech Republic;* orcid.org/0000-0001-9493-539X

Jaromír Vyhnanovský − *Institute of Analytical Chemistry of the Czech Academy of Sciences, 602 00 Brno, Czech Republic; Faculty of Science, Department of Analytical Chemistry, Charles University, 128 43 Prague, Czech Republic;* orcid.org/0000-0002-4635-0706

Ralph E. Sturgeon − *National Research Council of Canada, Ottawa, Ontario K1A 0R6, Canada;* orcid.org/0000-0001-7304-3034

Complete contact information is available at: https://pubs.acs.org/10.1021/acs.analchem.2c04660

Notes

The authors declare no competing financial interest.

ACKNOWLEDGMENTS

The work was supported by the Czech Science Foundation (projects 19-17604Y and 23-06530S), the Czech Academy of

Sciences (Institutional Research Plan RVO: 68081715) and Charles University (projects GAUK 60120 and SVV260560).

REFERENCES

(1) Anbar, A. D.; Wasserburg, G. J.; Papanastassiou, D. A.; Andersson, P. S. *Science* **1996**, *273*, 1524−1528.
(2) Fresco, J.; Weiss, H. V.; Phillips, R. B.; Askeland, R. A. *Talanta* **1985**, *32*, 830−831.
(3) Soyol-Erdene, T.-O.; Huh, Y.; Hong, S.; Hur, S. D. *Environ. Sci. Technol.* **2011**, *45*, 5929−5935.
(4) Rao, C. R. M.; Reddi, G. S. *TrAC, Trends Anal. Chem.* **2000**, *19*, 565−586.
(5) Cobelo-García, A.; Filella, M.; Croot, P.; Frazzoli, C.; Du Laing, G.; Ospina-Alvarez, N.; Rauch, S.; Salaun, P.; Schäfer, J.; Zimmermann, S. *Environ. Sci. Pollut. Res.* **2015**, *22*, 15188−15194.
(6) Rauch, S.; Hemond, H. F.; Peucker-Ehrenbrink, B. *Environ. Sci. Technol.* **2004**, *38*, 396−402.
(7) Komendova, R. *TrAC, Trends Anal. Chem.* **2020**, *122*, No. 115708.
(8) Sturgeon, R. E. *J. Anal. At. Spectrom.* **2017**, *32*, 2319−2340.
(9) Leonori, D.; Sturgeon, R. E. *J. Anal. At. Spectrom.* **2019**, *34*, 636−654.
(10) Yu, Y.; Hu, J.; Zhao, X.; Liu, J.; Gao, Y. *Anal. Bioanal. Chem.* **2022**, *414*, 5709−5717.
(11) Zhen, Y.; Chen, H.; Zhang, M.; Hu, J.; Hou, X. *Appl. Spectrosc. Rev.* **2022**, *57*, 318−337.
(12) Yang, Q.; Chen, H.; Hu, J.; Huang, K.; Hou, X. *Anal. Chem.* **2022**, *94*, 593−599.
(13) Musil, S.; Vyhnanovský, J.; Sturgeon, R. E. *Anal. Chem.* **2021**, *93*, 16543−16551.
(14) Sturgeon, R. E.; Pagliano, E. *J. Anal. At. Spectrom.* **2020**, *35*, 1720−1726.
(15) Vyhnanovský, J.; Sturgeon, R. E.; Musil, S. *Anal. Chem.* **2019**, *91*, 13306−13312.
(16) Šoukal, J.; Sturgeon, R. E.; Musil, S. *Anal. Chem.* **2018**, *90*, 11688−11695.
(17) de Oliveira, R. M.; Borges, D. L. G. *J. Anal. At. Spectrom.* **2018**, *33*, 1700−1706.
(18) de Oliveira, R. M.; Borges, D. L. G.; Grinberg, P.; Sturgeon, R. E. *J. Anal. At. Spectrom.* **2021**, *36*, 2097−2106.
(19) Hu, J.; Sturgeon, R. E.; Nadeau, K.; Hou, X.; Zheng, C.; Yang, L. *Anal. Chem.* **2018**, *90*, 4112−4118.
(20) Zhou, J.; Deng, D.; Su, Y.; Lv, Y. *Microchem. J.* **2019**, *146*, 359−365.
(21) Xu, F.; Zou, Z.; He, J.; Li, M.; Xu, K.; Hou, X. *Chem. Commun.* **2018**, *54*, 4874−4877.
(22) Vyhnanovský, J.; Yildiz, D.; Štádlerová, B.; Musil, S. *Microchem. J.* **2021**, *164*, No. 105997.
(23) Yu, Y.; Zhao, Q.; Bao, H.; Mou, Q.; Shi, Z.; Chen, Y.; Gao, Y. *Geostand. Geoanal. Res.* **2020**, *44*, 617−627.
(24) Mou, Q.; Dong, L.; Xu, L.; Song, Z.; Yu, Y.; Wang, E.; Zhao, Y.; Gao, Y. *J. Anal. At. Spectrom.* **2021**, *36*, 1422−1430.
(25) Gao, Y.; Xu, M.; Sturgeon, R. E.; Mester, Z.; Shi, Z.; Galea, R.; Saull, P.; Yang, L. *Anal. Chem.* **2015**, *87*, 4495−4502.
(26) Zeng, W.; Hu, Z.; Luo, J.; Hou, X.; Jiang, X. *Anal. Chim. Acta* **2022**, No. 339361.
(27) Zeng, W.; Hu, J.; Chen, H.; Zou, Z.; Hou, X.; Jiang, X. *J. Anal. At. Spectrom.* **2020**, *35*, 1405−1411.
(28) Xu, T.; Hu, J.; Chen, H. *Microchem. J.* **2019**, *149*, No. 103972.
(29) Hu, J.; Chen, H.; Jiang, X.; Hou, X. *Anal. Chem.* **2021**, *93*, 11151−11158.
(30) Wang, Y.; Lin, L.; Liu, J.; Mao, X.; Wang, J.; Qin, D. *Analyst* **2016**, *141*, 1530−1536.
(31) Yu, Y.; Jia, Y.; Shi, Z.; Chen, Y.; Ni, S.; Wang, R.; Tang, Y.; Gao, Y. *Anal. Chem.* **2018**, *90*, 13557−13563.
(32) He, H.; Peng, X.; Yu, Y.; Shi, Z.; Xu, M.; Ni, S.; Gao, Y. *Anal. Chem.* **2018**, *90*, 5737−5743.
(33) Nováková, E.; Horová, K.; Červený, V.; Hraníček, J.; Musil, S. *J. Anal. At. Spectrom.* **2020**, *35*, 1380−1388.
(34) Dong, L.; Chen, H.; Ning, Y.; He, Y.; Yu, Y.; Gao, Y. *Anal. Chem.* **2022**, *94*, 4770−4778.
(35) Hu, J.; Chen, H.; Hou, X.; Jiang, X. *Anal. Chem.* **2019**, *91*, 5938−5944.
(36) Jeníková, E.; Nováková, E.; Hraníček, J.; Musil, S. *Anal. Chim. Acta* **2022**, *1201*, No. 339634.
(37) Yu, Y.; Chen, H.; Zhao, Q.; Mou, Q.; Dong, L.; Wang, R.; Shi, Z.; Gao, Y. *Anal. Chem.* **2021**, *93*, 3343−3352.
(38) Cuello-Nuñez, S.; Abad-Álvaro, I.; Bartczak, D.; del Castillo Busto, M. E.; Ramsay, D. A.; Pellegrino, F.; Goenaga-Infante, H. *J. Anal. At. Spectrom.* **2020**, *35*, 1832−1839.
(39) Šoukal, J.; Musil, S. *Microchem. J.* **2022**, *172*, No. 106963.
(40) de Jesus, C. H.; Grinberg, P.; Sturgeon, R. E. *J. Anal. At. Spectrom.* **2016**, *31*, 1590−1604.
(41) Deng, H.; Zheng, C.; Liu, L.; Wu, L.; Hou, X.; Lv, Y. *Microchem. J.* **2010**, *96*, 277−282.
(42) Guo, X.; Sturgeon, R. E.; Mester, Z.; Gardner, G. *Appl. Organomet. Chem.* **2004**, *18*, 205−211.
(43) Zheng, C.; Sturgeon, R. E.; Brophy, C. S.; He, S.; Hou, X. *Anal. Chem.* **2010**, *82*, 2996−3001.
(44) Zheng, C.; Yang, L.; Sturgeon, R. E.; Hou, X. *Anal. Chem.* **2010**, *82*, 3899−3904.
(45) Gao, Y.; Sturgeon, R. E.; Mester, Z.; Pagliano, E.; Galea, R.; Saull, P.; Hou, X.; Yang, L. *Microchem. J.* **2016**, *124*, 344−349.
(46) Grinberg, P.; Mester, Z.; Sturgeon, R. E.; Ferretti, A. *J. Anal. At. Spectrom.* **2008**, *23*, 583−587.
(47) Grinberg, P.; Sturgeon, R. E.; Gardner, G. *Microchem. J.* **2012**, *105*, 44−47.
(48) Lopes, G. S.; Sturgeon, R. E.; Grinberg, P.; Pagliano, E. *J. Anal. At. Spectrom.* **2017**, *32*, 2378−2390.
(49) Weusten, S. J. C.; de Groot, M. T.; van der Schaaf, J. *J. Electroanal. Chem.* **2020**, *878*, No. 114512.
(50) Bings, N. H.; von Niessen, J. O. O.; Schaper, J. N. *Spectrochim. Acta, Part B* **2014**, *100*, 14−37.
(51) Hieber, W.; Lagally, H. *Z. Anorg. Allg. Chem.* **1940**, *245*, 321−333.
(52) Whyman, R. *J. Chem. Soc. D* **1969**, *23*, 1381−1382.
(53) Whyman, R. *J. Chem. Soc., Dalton Trans.* **1972**, 2294−2296.
(54) Pagliano, E.; Vyhnanovský, J.; Musil, S.; de Oliveira, R. M.; Forczek, S. T.; Sturgeon, R. E. *J. Anal. At. Spectrom.* **2022**, *37*, 528−534.
(55) *NIST Chemistry WebBook*. https://webbook.nist.gov/chemistry/name-ser/ (accessed 2023-01-12).
(56) Vobecký, M.; Jakůbek, J.; Bustamante, C. G.; Koníček, J.; Pluhař, J.; Pospíšil, S.; Rubáček, L. *Anal. Chim. Acta* **1999**, *386*, 181−189.
(57) Balcerzak, M. *Anal. Sci.* **2002**, *18*, 737−750.

https://doi.org/10.1021/acs.analchem.2c04660
Anal. Chem. XXXX, XXX, XXX−XXX

Supporting Information

Highly Efficient Photochemical Vapor Generation for Sensitive Determination of Iridium by Inductively Coupled Plasma Mass Spectrometry

Stanislav Musil,[a,*] Eva Jeníková [a,b] Jaromír Vyhnanovský,[a,b] and Ralph E. Sturgeon[c]

[a] Institute of Analytical Chemistry of the Czech Academy of Sciences, Veveří 97, 602 00 Brno, Czech Republic

[b] Charles University, Faculty of Science, Department of Analytical Chemistry, Hlavova 8, 128 43 Prague, Czech Republic

[c] National Research Council of Canada, 1200 Montreal Road, Ottawa, Ontario K1A 0R6, Canada

* Corresponding author; E-mail: stanomusil@biomed.cas.cz (S. Musil)

TABLE OF CONTENTS:

EXPERIMENTAL SECTION

Instrumentation. Sample solutions were introduced in a flow-injection (FI) mode into a stream of the reaction medium with the aid of an injection valve (0.5 mL sample volume). Delivery at an arbitrary flow rate to the photoreactor was undertaken using a peristaltic pump (Reglo Digital, Ismatec) which was also used to evacuate waste from the gas-liquid separator (GLS). All connecting tubing was made of PTFE (i.d. 1 mm) with the exception of the Tygon pump tubing. The high-efficiency flow-through photoreactor was a 19 W low-pressure mercury discharge lamp (Jitian Instruments Co., Beijing, China) internally fitted with three efficiently irradiated lengths of synthetic quartz tubing (total volume 0.72 mL) as well as two short quartz segments on either end of the photoreactor (≈0.25 mL) which serve as exterior inlet and outlet sample connection ports; these segments are not efficiently irradiated. The effluent was mixed with a flow of Ar carrier and directed to the GLS (15 mL internal volume), as described elsewhere.[1,2] The outlet of the GLS was connected via PTFE tubing (2 mm i.d. x 40 cm long) to an Agilent 8900 ICPMS/MS via an ultra-high matrix introduction (UHMI) port located downstream of the Scott double-pass spray chamber of the ICPMS. This port is originally intended for on-line dilution of aerosols of samples with high salt content. Carrier liquid (2% HNO_3), mixed with an internal standard (IS) solution of 10 μg L^{-1} Re in 2% HNO_3, was concurrently introduced into the spray chamber via a MicroMist nebulizer (Burgener Research Inc., Mississauga, Canada). The liquid carrier channel was equipped with a manual injection valve (0.5 mL sample loop volume) and this arrangement was exclusively utilized for estimation/determination of overall PVG efficiency (see Section "Procedure and Conventions"). A schematic of the PVG system coupled to ICPMS is depicted in Figure S1.

No special cleaning of the photoreactor was necessary between sequential measurements and the chemifold was typically only flushed with DIW at the end of the measurement day. From time to time, the quartz photoreactor was manually filled with concentrated HNO_3 via a syringe and the UV lamp was powered on to initiate decomposition of HNO_3 and to facilitate dissolution and removal of any deposited (metal) impurities.

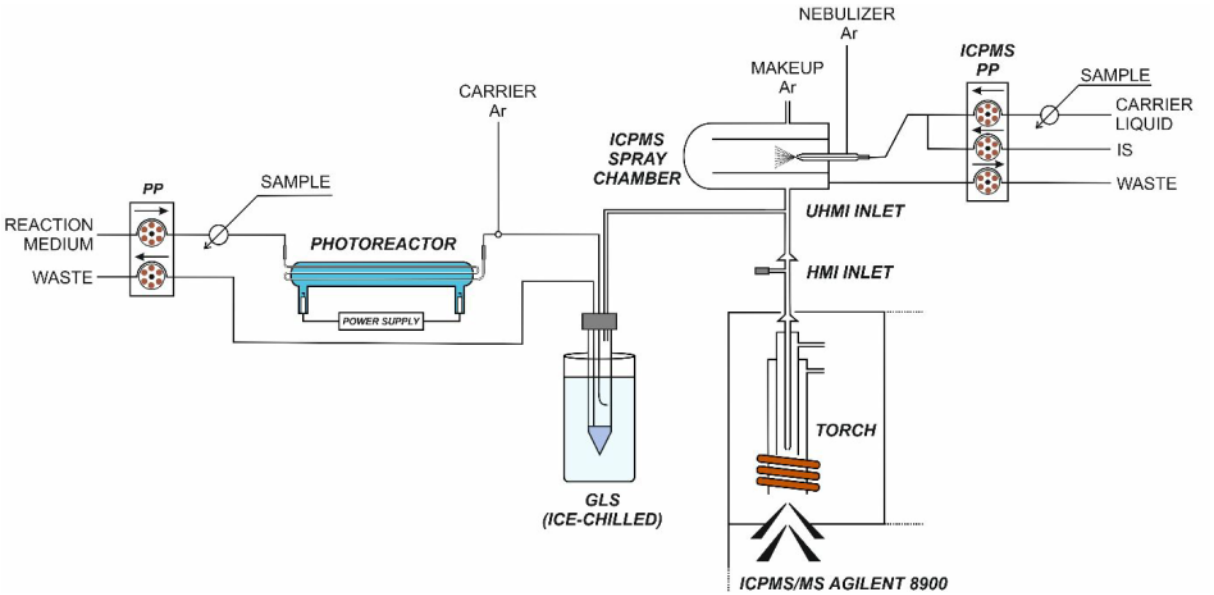

Figure S1. PVG arrangement for FI coupling to ICPMS with simultaneous liquid nebulization, GLS – gas-liquid separator, UHMI – ultra-high matrix introduction port.

Detection of generated volatile Ir species was achieved using an Agilent 8900 triple quadrupole ICPMS employing "wet plasma" conditions created by simultaneous pneumatic nebulization (PN) of a carrier liquid (2% HNO_3) mixed on-line with the IS solution.[1-4] More robust conditions are created in the ICP and this setup permits the monitoring/correction for any sensitivity drift due to changes in the plasma or interface transmission efficiency by means of the response changes noted for the nebulized IS.

Optimal plasma settings of the Agilent 8900 ICPMS/MS for coupling with PVG are summarized in Table S1. Isotopes ^{185}Re (IS, dwell time 0.05 s), ^{191}Ir (0.1 s) and ^{193}Ir (0.1 s) were always monitored and accompanied by ^{55}Mn (0.001 s), ^{56}Fe (0.001 s), ^{59}Co (0.001 s), ^{63}Cu (0.001 s), ^{103}Rh (0.05), ^{105}Pd (0.05), ^{111}Cd (0.001 s), ^{192}Pt (0.05 s) or ^{194}Pt (0.05 s) according to the actual demands during the optimization or real sample analysis. The transient FI signals were exported to, and integrated with, MS Excel and corrected for any sensitivity drift relative to changes in the co-introduced ^{185}Re IS signal intensity.

Table S1. Typical ICPMS/MS (Agilent 8900) parameters for coupling with PVG

RF power	1550 W
RF matching	1.4 V
Sampling depth	8.0 mm
Nebulizer Ar	960 mL min^{-1}
Makeup Ar	0 mL min^{-1}
Carrier Ar for PVG	200 mL min^{-1}
ICPMS peristaltic pump flow	0.1 rps (0.33 mL min^{-1} carrier liquid, 0.06 mL min^{-1} IS)
Spray chamber temperature	2 °C
Reaction/collision cell mode	No gas or He (4.1 mL min^{-1})
Acquisition mode	Time-resolved analysis
Scan type	Single quad
Measured isotopes (dwell time, s)[a]	^{191}Ir (0.1), ^{193}Ir (0.1), ^{185}Re (IS, 0.05)

[a] other isotopes, in addition to the default ones, monitored during the optimization or real sample analysis included: ^{55}Mn (0.001 s), ^{56}Fe (0.001 s), ^{59}Co (0.001 s), ^{63}Cu (0.001 s), ^{103}Rh (0.05), ^{105}Pd (0.05), ^{111}Cd (0.001 s), ^{192}Pt (0.05 s) or ^{194}Pt (0.05 s)

Conventional PN-ICPMS/MS equipped with an Agilent SPS 4 autosampler was employed for comparative determination of Ir in SRM NIST 2556 (Used Auto Catalyst) after peroxide fusion as well as of real water samples and to evaluate LODs for comparison with those by PVG. Five replicate steady-state measurements were acquired using a standard no gas mode and He mode (4.1 mL min^{-1}) of the collision cell. The gas flow, MS settings and measured isotopes are summarized in Table S2.

Table S2. ICPMS/MS parameters for conventional PN sample introduction

RF power	1550 W
RF matching	1.2 V
Sampling depth	8.0 mm
Nebulizer Ar	600 mL min^{-1}
Dilution Ar (UHMI)	550 mL min^{-1}
ICPMS peristaltic pump flow	0.1 rps (0.33 mL min^{-1} carrier liquid, 0.06 mL min^{-1} IS)
Spray chamber temperature	2 °C
Reaction/collision cell mode	No gas and He (4.1 mL min^{-1})
Acquisition mode	Spectrum (5 replicates)
Scan type	MS/MS (narrow peak)
Measured isotopes (dwell time, s)	^{191}Ir (0.3), ^{193}Ir (0.3), ^{101}Ru (IS, 0.1), ^{185}Re (IS, 0.1)

RESULTS AND DISCUSSION

Release and Transport of Volatile Species. The effect of argon (chemifold) carrier flow on the release and transport of volatile species to the ICPMS was examined using a reaction medium of 10 M HCOOH and sample flow rate of 1.5 mL min^{-1}. The gas stream leaving the GLS was mixed with an additional flow of argon (not shown in Figure S1) before it was introduced to the ICPMS. Care was taken to keep the total gas flow to the ICP the same, so as not to influence conditions in the plasma or sampling depth. Although a slightly lower peak area sensitivity (by 9%) was obtained at 50 mL min^{-1} supplied to the GLS, no significant further effect of carrier Ar for PVG was observed in the range 100−600 mL min^{-1}, suggesting an efficient release and stability of the gaseous product. A flow rate of 200 mL min^{-1} was chosen as optimal in order to minimize any potential load of HCOOH vapor on the ICP.

The efficiency of release of volatile species from the liquid reaction medium was also investigated. The GLS was operated in such way that no liquid comprising the sample was maintained in the GLS (the PTFE tube for waste removal was moved to the bottom of the GLS) and the peak area sensitivities were compared to those obtained with the GLS operated with 1.5 mL of the reaction medium maintained inside the GLS. No significant changes in peak area sensitivity using 10 M HCOOH as the reaction medium were identified between either setup for sample flow rates of 1, 1.5 and 2.5 mL min^{-1}. This result suggests that the majority of the volatile Ir species is released to the gas phase upstream of the GLS, most probably after mixing with carrier Ar in the short transfer line to the GLS (see Figure S1). The chilling of the GLS in an ice-water bath also had no impact on peak area sensitivity but was used throughout as it significantly limited carryover of small droplets of the reaction medium formed in the GLS to the transport tube connected to the ICP and thus improved stability of measured signals.

PVG without Additives

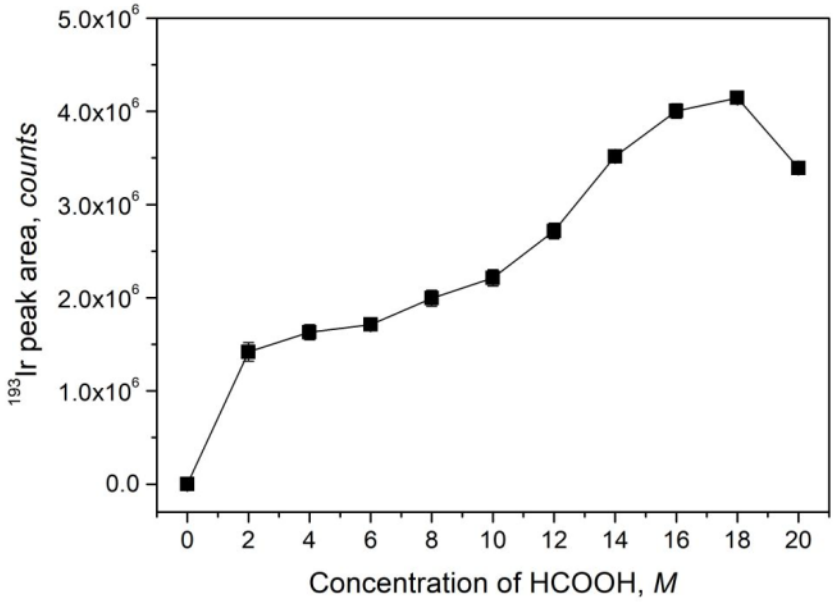

Figure S2. Influence of HCOOH concentration on peak area response from 200 ng L^{-1} Ir^{3+} at a sample flow rate of 1.5 mL min^{-1}. Uncertainties expressed as SD in some cases are sufficiently small that they cannot be discerned from the data points.

Effect of pH

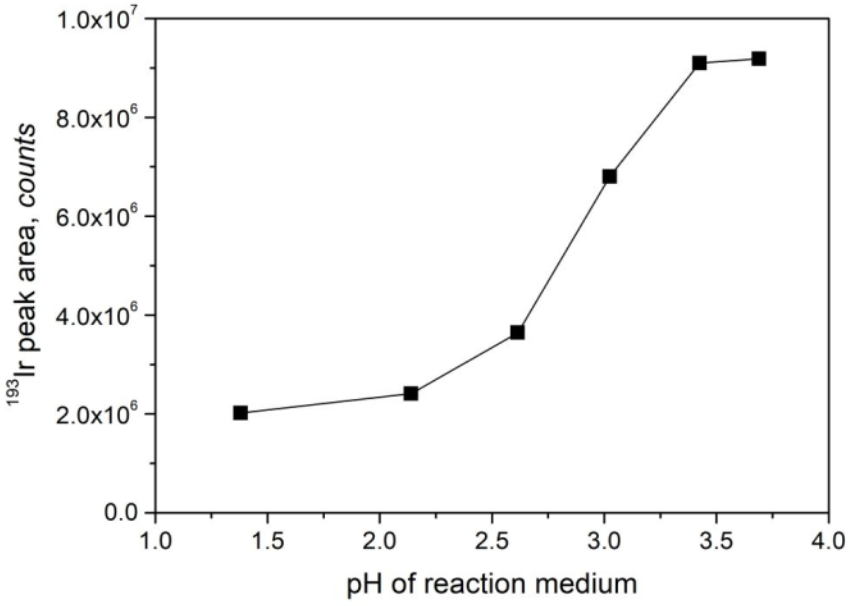

Figure S3. Effect of pH of reaction medium investigated by varying the volume of liquid $NH_3{\cdot}H_2O$ added to 10 M HCOOH on peak area response from 200 ng L^{-1} Ir^{3+}, sample flow rate of 1.5 mL min^{-1}. Uncertainties expressed as RSD in all cases are lower than 1.5%.

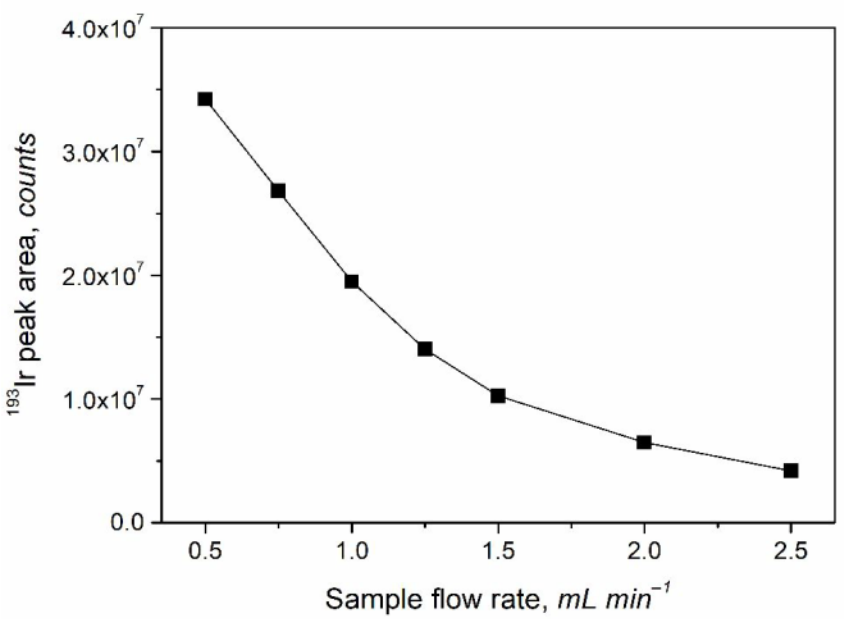

Figure S4. Effect of sample flow rate at pH = 3.4 of the reaction medium prepared by addition of liquid $NH_3 \cdot H_2O$ to 10 M HCOOH on peak area response from 200 ng L^{-1} Ir^{3+}. Uncertainties expressed as RSD in all cases are lower than 1.5%.

PVG with Metal Ion Sensitizers

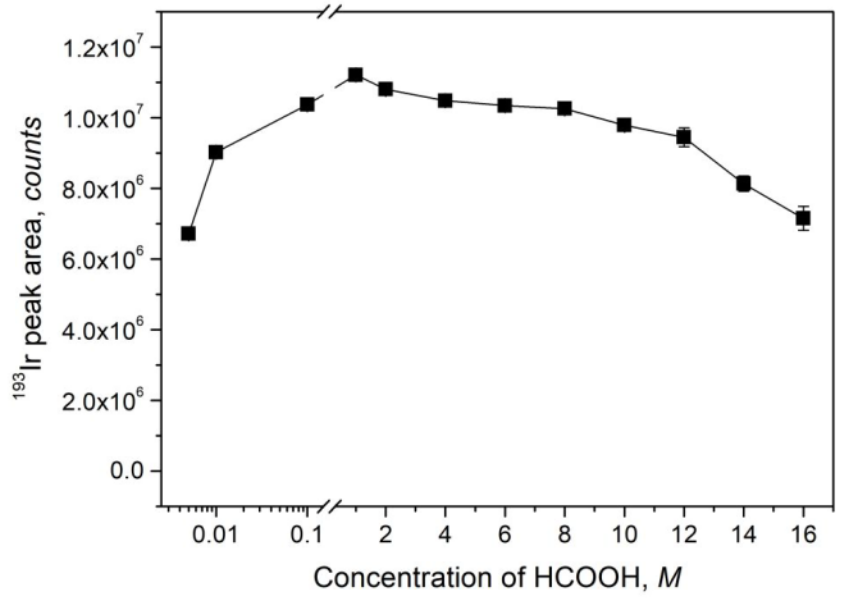

Figure S5. Influence of HCOOH concentration on peak area response from 50 ng L^{-1} Ir^{3+} using 10 mg L^{-1} Co^{2+} and 25 mg L^{-1} Cd^{2+} as sensitizers at a sample flow rate of 1.5 mL min^{-1}. The range 0.0025 M to 0.15 M given in logarithmic scale. Uncertainties expressed as SD in some cases are sufficiently small that they cannot be discerned from the data points.

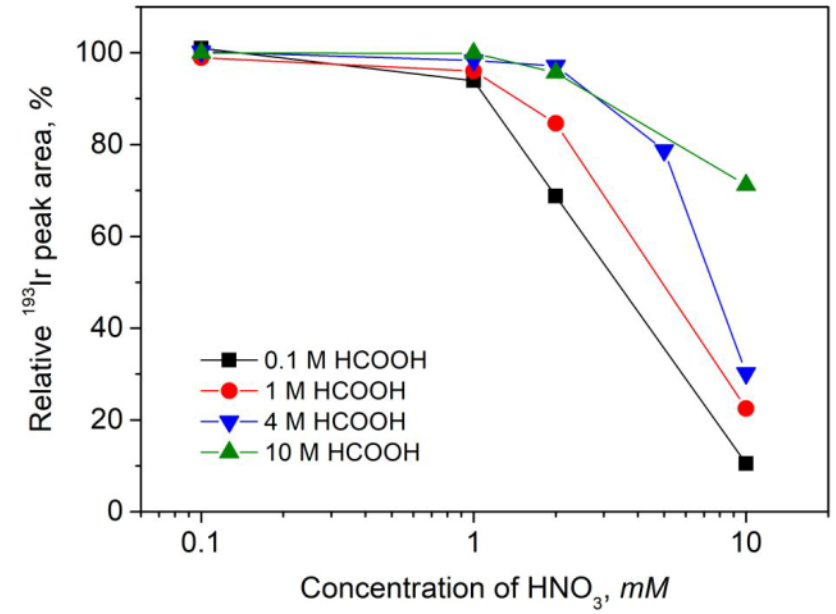

Figure S6. Relative effects of added HNO_3 on PVG from 50 ng L^{-1} Ir^{3+} in various HCOOH media containing 10 mg L^{-1} Co^{2+} and 25 mg L^{-1} Cd^{2+} as sensitizers. Combined uncertainty in all cases is lower than 2%.

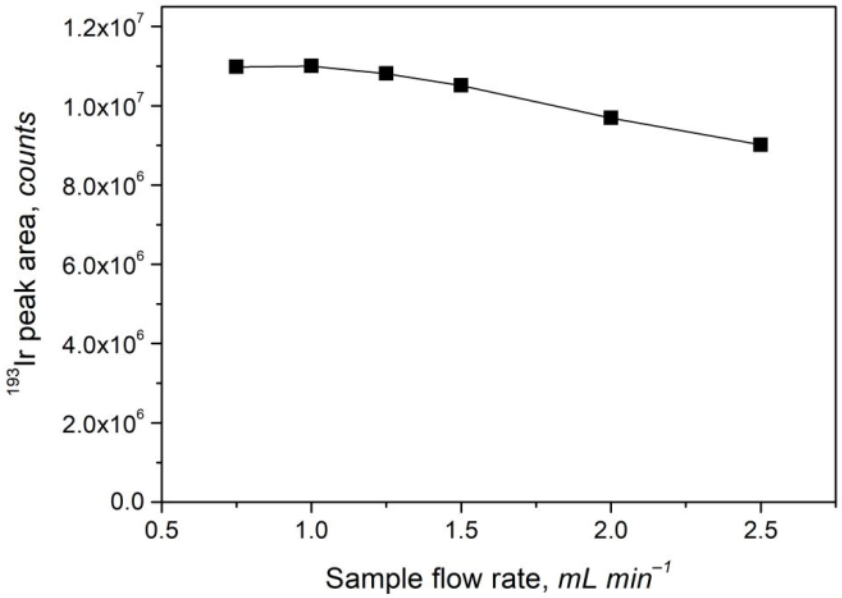

Figure S7. Effect of sample flow rate using 10 mg L^{-1} Co^{2+} and 25 mg L^{-1} Cd^{2+} as sensitizers in 4 M HCOOH on peak area response from 50 ng L^{-1} Ir^{3+}. Uncertainties expressed as RSD in all cases are lower than 2%.

Table S3. Influence of various co-existing ions (expressed as % recovery)[a] on Ir response (50 ng L^{-1}) examined by FI-PVG-ICPMS

Interferent	Concentration (mg L^{-1}) [interferent/analyte]			
	0.01 [200]	0.1 [2,000]	1 [20,000]	10 [200,000]
Mn^{2+}	98	99	99	99
Fe^{3+}	98	99	98	101
Cu^{2+}	99	97	80	91
Zn^{2+}	99	100	100	99
As^{3+}	98	90	30	1
Se^{4+}	100	92	69	25
Mo^{6+}	99	101	99	99
Pt^{4+}	100	93	64	34
Au^{3+}	99	100	58	13

[a] relative combined uncertainty (combined uncertainty/recovery) is <2% for all recovery values

REFERENCES

(1) Vyhnanovský, J.; Sturgeon, R. E.; Musil, S. Cadmium Assisted Photochemical Vapor Generation of Tungsten for ICPMS detection. *Analytical Chemistry* **2019**, *91*, 13306-13312.

(2) Vyhnanovský, J.; Yildiz, D.; Štádlerová, B.; Musil, S. Efficient photochemical vapor generation of bismuth using a coiled Teflon reactor: Effect of metal sensitizers and analytical performance with flame-in-gas-shield atomizer and atomic fluorescence spectrometry. *Microchemical Journal* **2021**, *164*, 105997.

(3) Musil, S.; Vyhnanovsky, J.; Sturgeon, R. E. Ultrasensitive Detection of Ruthenium by Coupling Cobalt and Cadmium Ion-Assisted Photochemical Vapor Generation to Inductively Coupled Plasma Mass Spectrometry. *Analytical Chemistry* **2021**, *93*, 16543-16551.

(4) Šoukal, J.; Sturgeon, R. E.; Musil, S. Efficient Photochemical Vapor Generation of Molybdenum for ICPMS Detection. *Analytical Chemistry* **2018**, *90*, 11688-11695.